FRONTIERS OF PHYSICS

TOPICAL REVIEW
Volume 19 / Issue 2 / 24302 / 2024

Investigations of nuclear chirality at iThemba LABS

R. A. Bark[1,†], E. A. Lawrie[1], C. Liu[2], S. Y. Wang[2]

1 iThemba Laboratory for Accelerator Based Sciences, National Research Foundation, P.O. Box 722, Somerset-West 7129, South Africa
2 Shandong Provincial Key Laboratory of Optical Astronomy and Solar-Terrestrial Environment, Institute of Space Sciences, Shandong University, Weihai 264209, China
Corresponding author. E-mail: †ra.bark@ilabs.nrf.ac.za
Received March 16, 2023; accepted August 5, 2023

ABSTRACT

Progress in the studies of chirality in atomic nuclei at iThemba LABS is reviewed. New regions of chirality, around mass 80 and 190 have been discovered using the AFRODITE array, specifically in the nuclei ^{74}As, ^{78,80,82}Br, ^{81}Kr, and ^{193,194,198}Tl. Many phenomena have been observed, including multiple chiral bands in the same nucleus, the coexistence of octupole correlations and nuclear chirality, and the coexistence of pseudo spin and nuclear chirality. The best example of chiral degeneracy to date, was found in ^{194}Tl. The level scheme of ^{106}Ag has been revisited and interpreted in terms of two- and four-quasiparticle bands. Investigations using the particle-rotor model have shown that the fingerprints of chirality in the two-quasiparticle system only can occur in an idealised model description that is unrealistic. For systems with a higher number of quasiparticles, the calculations showed that nuclear chirality can persist.

Keywords chirality, high-spin states, particle-rotor model

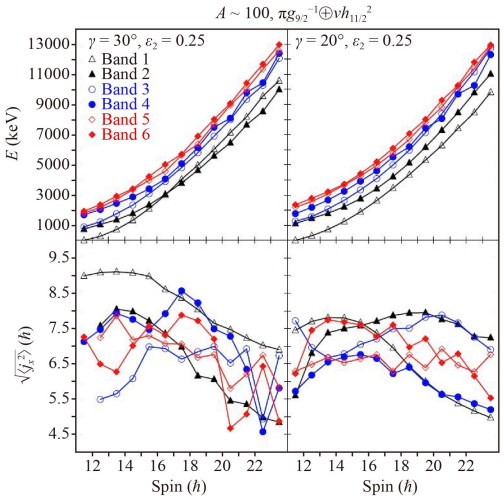

Contents

*Special Topic: Nuclear Chirality over the Past 25 Years (Eds. Qibo Chen & Pengwei Zhao).

Higher Education Press

https://doi.org/10.1007/s11467-023-1340-0

1 Introduction

In their seminal paper, Frauendorf and Meng [1] showed that there were specific nuclear configurations that, in the particle-rotor model, would give rise to rotational bands having a very special feature - beyond a given critical spin, the bands would form degenerate pairs. The calculated excitation energies for such bands are shown in Fig. 1. They are based on the $\pi h_{11/2} \otimes \nu h_{11/2}^{-1}$ configuration, with a triaxial nuclear shape and triaxiality parameter $\gamma = 30°$. Near their band heads the yrast and the first excited rotational bands differ considerably in their excitation energies for the same spin I, but as the angular momentum in both bands increases, the relative excitation energy diminishes, until, beyond a critical spin, (in this case $I_c \sim 13\hbar$), the two bands become degenerate. Beyond this critical spin not only the excitation energies but all features of the bands become identical, including moments-of-inertia, alignments, intra-band $B(M1)$ and $B(E2)$ transition probabilities, etc. The next pair of excited bands calculated for the same configuration was found to behave in a similar way, that is, the two bands have different excitation energies (and other features) near their band heads, but become degenerate above a certain critical angular momentum (in this case $I_c \sim 16\hbar$).

This striking behaviour of the calculated bands was found for nuclei with triaxial shape and for nuclear configurations built on two valence nucleons, where one of the nucleons occupied a single-particle orbital near the bottom of a shell (in this case the proton occupied the lowest-energy orbital of the $h_{11/2}$ shell), while the other was placed in an orbital near the top of a shell (in this case the neutron occupied the highest-energy orbital of the $h_{11/2}$ shell). The observed degeneracy was explained by Frauendorf and Meng [1] as due to the chiral symmetry formed in angular momentum space. It is known that the angular momentum of a valence nucleon (i) at the bottom of the shell is oriented along the short nuclear axis, (ii) at the top of a shell is oriented along the long nuclear axis, and the angular momentum of a rotating triaxial core is predominantly aligned along the intermediate axis. Therefore, in such a system these three angular momenta are mutually orthogonal, and can form both a left- and a right-handed systems, as illustrated in Fig. 1. As both the left and the right-handed systems formed in the intrinsic frame of the nucleus (defined by the three nuclear axes) are in many ways identical, two rotational bands with identical features will be observed in the laboratory frame. These degenerate chiral partner bands will have the same excitation energies and $B(M1)$ and $B(E2)$ transition probabilities. For a system with a chiral geometry the total angular momentum is out-of-plane, that is out of the planes defined by any two major nuclear axes.

The search for degenerate pairs of chiral bands

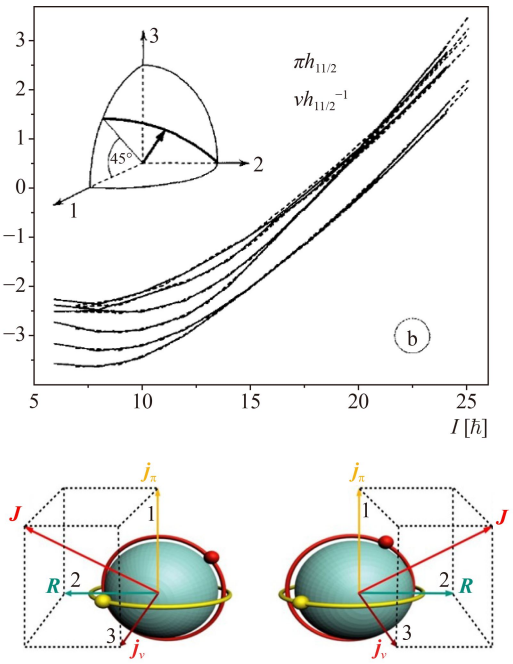

Fig. 1 Top: Excitation energies calculated with the PRM for a triaxial nucleus with $\gamma = 30°$ and with nucleon configuration $\pi h_{11/2} \otimes \nu h_{11/2}^{-1}$ [1]. Bottom: A sketch illustrating the left- and right-handed systems formed in angular momentum space by the angular momenta of the valence proton, j_π, of the valence neutron, j_ν and of the rotation, R.

became a new hot topic in nuclear structure. iThemba LABS became an international centre for the study of chirality by local and visiting groups from China, with the principal experimental facility being the AFRODITE array of HpGe detectors, coupled to the Separated Sector Cyclotron. This led to the exploration of existing and new regions of chirality on the nuclear chart, chiefly using the methods of in-beam γ-ray spectroscopy. Theoretical and experimental questions focussed on testing the predicted features of chiral partner bands, including (i) why the bands would become degenerate only above a critical spin I_c, (ii) would the experimentally observed bands be truly degenerate and if not, what would affect how strongly the degeneracy is broken, (iii) would there be other fingerprints of chiral geometry, (iv) what would be the impact of the single-particle angular momenta, e. g. would it be possible to have chiral systems where the single-particle angular momenta on the short and long axes are very different. The investigations would soon lead to unexpected discoveries relating chirality to other symmetries such as pseudo spin and reflection asymmetry.

This topic covered in this article is divided into the following sections: Section 2 Theoretical studies of chiral systems at iThemba LABS; Section 3 Experimental techniques; Section 4 New Regions of Chirality; Section 5 Close near-degeneracy and multiple bands; Section 6

Resolution of a chiral conundrum in the mass 100 region; Section 7 Pseudo spin and reflection asymmetry.

2 Theoretical studies of chiral systems at iThemba LABS

2.1 Degeneracy in chiral partner bands

Among all chiral systems observed to date, [2], there are no chiral partner bands that are truly degenerate in their excitation energies, alignments, energy staggering patterns, $B(M1)$ and $B(E2)$ transition probabilities. Thus, it is important to understand what causes the differences in the properties of the chiral partner bands.

Frauendorf and Meng [1] understood that the difference in the excitation energies in the calculated partner bands of Fig. 1 at low angular momenta ($I < I_c$) were a result of a planar geometry of the angular momenta, where the total angular momentum remained oriented in the plane of the short – long axes (the plane defined by axes 1 and 3 in Fig. 1). Only above a critical I_c would the rotational angular momentum along the intermediate axis become sufficiently large to flip the total angular momentum I away from that plane into an aplanar orientation (where I has considerable components along all three nuclear axes) and a chiral geometry be formed in angular momentum space. But what may cause the divergence from degeneracy for $I > I_c$? It was naturally expected that such divergence might be caused by features of the shape of the nucleus, for instance the shape might not correspond to largest non-axiality with $\gamma = 30°$, or that it may possess some γ softness, that may trigger mixtures and overlaps of the wave functions of the left- and right-handed systems.

Lawrie and Shirinda [3] studied further the features of chiral bands, using the two-quasiparticle-triaxial-rotor model (QTR) [4, 5]). They noted that when the wave functions of the left- and right-handed systems are not perfectly orthogonal but have some small overlap, the expectation values of all the relevant operators such as those of the excitation energies, single-particle, rotational and total angular momenta, $B(M1)$ and $B(E2)$ transition probabilities, etc., would show non-identical values for the chiral partner bands. Thus, if any divergence from degeneracy would appear, it would be present in all properties of the chiral partner bands. The magnitudes of the divergences in the properties of the chiral partner bands were then studied. Most importantly the impacts of (i) the triaxiality γ, and (ii) nucleon configurations, were evaluated. The calculated relative excitation energies of chiral bands with the $\pi h_{11/2} \otimes \nu h^{-1}_{11/2}$ configuration (where the proton and the neutron occupied the lowest- and highest-energy orbitals of the $h_{11/2}$ shell), at a quadrupole deformation of $\varepsilon_2 = 0.15$, for three different cases of chiral systems are shown in Fig. 2. For each of these cases the calculated total angular momentum is

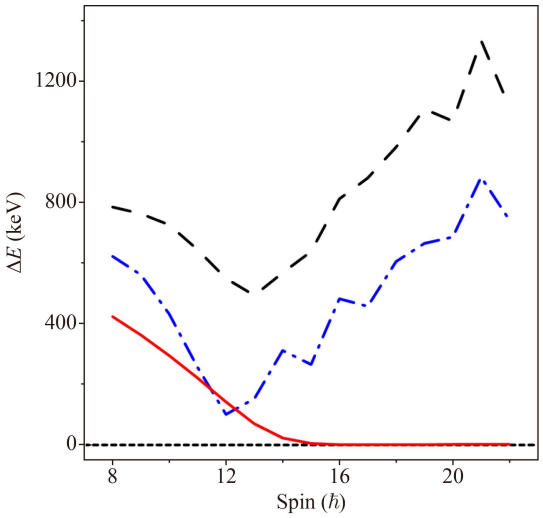

Fig. 2 Calculated [3] relative excitation energy for the $\pi h_{11/2} \otimes \nu h^{-1}_{11/2}$ chiral bands, $\Delta E = E_{side} - E_{yrast}$, for $\varepsilon_2 = 0.15$ and for three different cases. The solid red line corresponds to $\gamma = 30°$ and fixed single-particle angular momenta of both valence nucleons, (e.g., j_π and j_ν are fixed along the short and long nuclear axes, respectively). The dashed–dotted blue line corresponds to $\gamma = 30°$, the same Fermi levels for protons and neutrons, but allowing their configuration spaces to span over 5 single-particle orbitals each. The dashed black line corresponds to $\gamma = 20°$ and the same configuration space of 5 orbitals, for protons and neutrons.

aplanar (with considerable projections along the three nuclear axes), and thus chiral systems are formed.

When, at $\gamma = 30°$, the single-particle angular momenta j_π and j_ν are fixed and aligned along the short ($\Omega_\pi = 11/2$) and long ($\Omega_\nu = 11/2$) nuclear axes by restricting the configuration spaces for protons and neutrons to one orbital each, the chiral bands reach degeneracy in their excitation energies above $I_c = 16\hbar$, (see the red curve in Fig. 2). Similarly degeneracy is reached for the other properties of these bands, such as projections of the angular momenta, $B(M1)$ and $B(E2)$ transition probabilities [3]. However, in realistic calculations the single-particle component of the wave function is a mixture of orbitals, which reflects the gradual alignment of the single-particle angular momenta under the influence of the Coriolis interaction. In a more realistic case which allows the configuration spaces for the proton and neutron to span five orbitals near the corresponding Fermi levels, the calculated chiral partner bands do not reach degeneracy, as shown by the dashed-dotted blue curve in Fig. 2. Instead there is a considerable divergence in the excitation energies (and all other features of the chiral partner bands). The impact of the nucleon configuration space is thus significant. The effect induced by a reduction of the triaxial deformation to $\gamma = 20°$ seems to be somewhat smaller (compare the difference between the dashed black and the dashed–dotted blue curves with that between the dashed–dotted blue and red

curves in Fig. 2).

Therefore, it was concluded that chiral partner bands in real nuclei are not expected to show degeneracy, but only a certain degree of similarity in their properties, which is often referred to as near-degeneracy. The expectation that chiral partner bands would show degeneracy in their excitation energies and other features is based on an idealistic theoretical description that assumes that the single-particle angular momenta that are fixed and remain fully aligned along the long and short axes.

These studies also noted that the expectation value of the angles between the three angular momenta, $\alpha(j_\pi, j_\nu)$, $\alpha(j_\pi, R)$, and $\alpha(j_\nu, R)$, remain very close to 90° for both chiral partner bands and for $\gamma = 30°$ only in the case of configuration spaces restricted to one orbital, see the red curves in Fig. 3. In more realistic calculations that involve larger configuration spaces, these angles tend to decease at higher spins. These results imply that the typical sketch illustrating the nuclear chiral system as built of three mutually orthogonal angular momenta (e.g., Fig. 1) is simplified. In real nuclei the average angles between the angular momenta of the proton, neutron and collective rotation are smaller and decrease further at higher spins.

The calculated wave functions for the chiral partner bands were further investigated [6], in order to understand better the orientation of the three angular momenta. While the average angles $\alpha(j_\pi, j_\nu)$, $\alpha(j_\pi, R)$, and $\alpha(j_\nu, R)$, suggested an aplanar orientation of the total angular momentum and a chiral geometry (see Fig. 3), it was interesting to determine whether there were contributions with non-chiral, planar orientation of the total angular momentum. Such components of the wave function would have vanishing projection of the total angular momentum along one of the nuclear axes and their presence would cause a loss of degeneracy in the chiral partner bands.

The probabilities for vanishing projection of the total angular momentum along the three nuclear axes and for the two partner bands are shown in Fig. 4. Consider the case of triaxial deformation with $\gamma = 30°$, and restricted to one orbital configuration spaces, shown in magenta diamonds in Fig. 4. At low spins ($I < 16\hbar$), there are negligible contributions with vanishing projections of I along the short and long nuclear axes; however, there is a considerable component with vanishing projection along the intermediate axis, which causes the lack of degeneracy in the chiral partners, see Fig. 2. Note that as this contribution decreases at higher spins, the similarity in the properties of the partner bands improves and degeneracy is established for $I > 16\hbar$, see Fig. 2. Indeed, for $I > 16\hbar$ the contributions of components with non-chiral geometry (with $I_s = 0$, $I_i = 0$, and $I_l = 0$), are negligible ($< 2\%$), see Fig. 4.

It can be noted that for realistic configurations, where the single-particle angular momenta are not fixed along

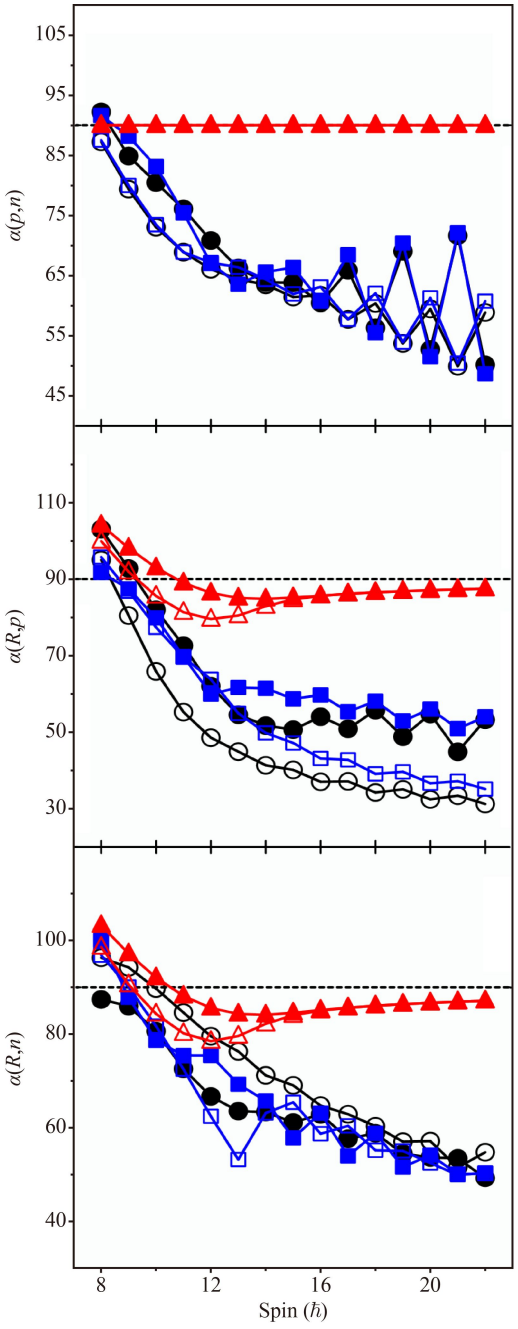

Fig. 3 Calculated expectation values for the angles between the angular momenta j_π, j_ν and R, for the $\pi h_{11/2} \otimes \nu h_{11/2}^{-1}$ chiral bands, for $\varepsilon_2 = 0.15$, and for three cases of chiral bands, as described in Fig. 2 and in the text. The data for the yrast and side chiral bands are denoted with open and filled symbols, respectively. The red triangles correspond to $\gamma = 30°$, and proton and neutron restricted to the lowest- and highest-energy orbitals of the $h_{11/2}$ shell only – i.e. where j_π and j_ν are fixed along the short and long nuclear axes, respectively. The blue squares correspond to $\gamma = 30°$, the same Fermi levels for protons and neutrons, but allowing their corresponding configuration spaces to span over 5 single-particle orbitals. The black circles correspond to $\gamma = 20°$ and the same configuration spaces of 5 orbitals for protons and neutrons. Reproduced from Ref. [6].

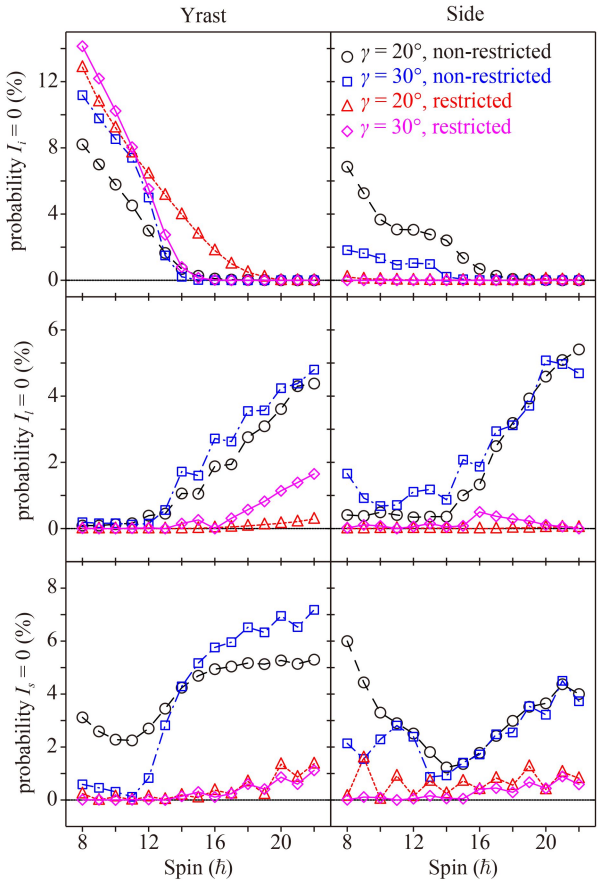

Fig. 4 Calculated probability for vanishing projection of the total angular momentum along the short (s), intermediate (i), and long (l) axes for the $\pi h_{11/2} \otimes \nu h_{11/2}^{-1}$ chiral partner bands and for restricted (fixed single-particle angular momenta) and non-restricted (free single-particle angular momenta) configurations and for $\varepsilon_2 = 0.15$. Reproduced from Ref. [6].

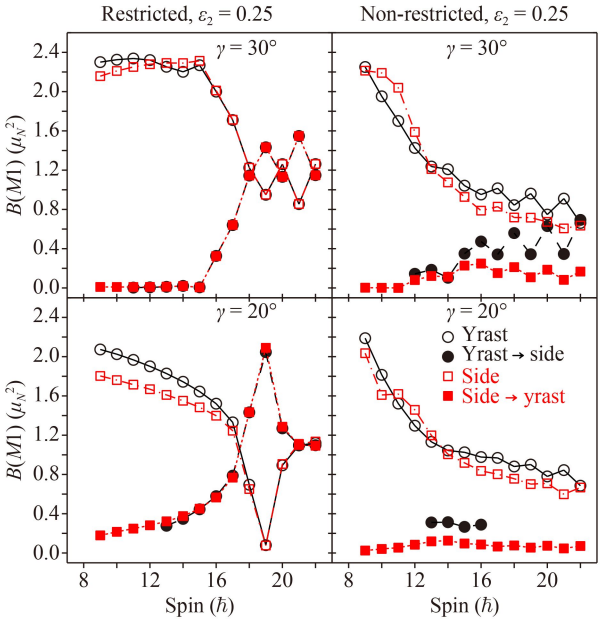

Fig. 5 Calculated intra- and inter-band $B(M1)$ transition probabilities for the $\pi h_{11/2} \otimes \nu h_{11/2}^{-1}$ chiral partner bands, with fixed single-particle angular momenta (restricted configuration space) and free single-particle angular momenta (non-restricted configuration space) at $\varepsilon_2 = 0.25$. Open and filled symbols denote intra- and inter-band $B(M1)$ rates, respectively. Reproduced from Ref. [6].

the nuclear axes, the calculated lack of degeneracy for higher spins is caused by contributions corresponding to non-chiral geometry (with $I_s = 0$, and $I_l = 0$). The predicted considerable loss of degeneracy in the properties of the chiral partner bands is caused by relatively small planar contributions; such contributions are typically less than 10%.

2.2 Other fingerprints of chiral symmetry

It is important to define clear fingerprints of chiral systems in nuclei. Indeed a chiral system with fixed single-particle angular momenta would create two degenerate rotational bands built on the same nucleon configuration. However, as discussed above, such expectations are unrealistic; a realistic description allows the single-particle angular momenta to change orientation under the influence of the Coriolis force. Such a description shows the expected degeneracy is lost and the two partner bands differ in all their properties, such as excitation energies, alignments, moments-of-inertia, and $B(M1)$ and $B(E2)$ transition probabilities. Furthermore, even small contributions from non-chiral components cause a substantial loss of degeneracy. Therefore, bands that correspond to a dominant chiral geometry of the angular momenta may show partner bands exhibiting considerable differences. This makes it important to search for additional fingerprints that can be used to identify chiral symmetry. Two additional fingerprints were proposed, (i) a specific staggering of the $B(M1)$ transition probabilities [7], and (ii) a lack of energy staggering in the rotational bands [8].

Shirinda and Lawrie investigated these two fingerprints further, in particular considering both ideal and realistic $\pi h_{11/2} \otimes \nu h_{11/2}^{-1}$ configurations [6]. They found that as in previous studies [7], the $B(M1)$ transition probabilities exhibit a large-magnitude staggering with a specific phase (high values for even spins for the intra-band transitions) particularly for the ideal case with $\gamma = 30°$ (for example see Fig. 5), which may weaken and disappear for less triaxial nuclear shape with $\gamma = 20°$. However, the calculations based on a realistic treatment of the nucleon configuration produced a very different result. They showed that even for the largest triaxiality of $\gamma = 30°$, the expected staggering patterns change. For instance, the staggering in the $B(M1)$ values may disappear, as observed for the intra-band transitions of the side band, or may even appear with opposite phase (low

values for even spins), as found for the intra-band transitions of the yrast band. The possible reasons for this changed behaviour were associated with the complexity of the $B(M1)$ rates and the number of factors that can influence them. For instance, in realistic calculations there is a strong staggering in the angles between the angular momenta (e.g., see the staggering in $\alpha(j_\pi, j_\nu)$ in Fig. 3). Therefore, it was concluded that the $B(M1)$ staggering cannot be considered as an unambiguous fingerprint of chirality, as other effects can overcome and change the staggering pattern expected for a chiral geometry.

It had been argued that chiral bands should not show energy staggering, because for a system with three mutually orthogonal angular momenta the Coriolis interaction would vanish [8]. On the other hand, as illustrated in Fig. 3 the angles between the three angular momenta are approximately 90° only for configuration spaces restricted to one nucleon orbital. These angles are much smaller and suggest considerable Coriolis effects when a realistic configuration space is considered.

To study further the energy staggering pattern as a possible fingerprint of chiral systems Shirinda and Lawrie [6] plotted the calculated energy staggering

$$S(I) = \frac{E(I) - E(I-1)}{2I} \tag{1}$$

for the $\pi h_{11/2} \otimes \nu h_{11/2}^{-1}$ chiral bands and $\gamma = 30°$ assuming $\varepsilon_2 = 0.15$ and $\varepsilon_2 = 0.25$, see Fig. 6. Indeed, for a chiral system with fixed-single particle angular momenta, the parameter $S(I)$ does not show staggering (see the magenta diamonds in Fig. 6). However, large energy staggering was found in both bands when a realistic description of the single-particle angular momenta was adopted at $\varepsilon_2 = 0.15$. This result was understood as a natural consequence of the Coriolis interaction acting on a system where the three angular momenta are not mutually orthogonal. This idea was further tested with calculations carried out for larger quadrupole deformation of $\varepsilon_2 = 0.25$. For the latter system the Coriolis interaction would be smaller due to the larger moment-of-inertia associated with the larger ε_2. Indeed the calculated parameter $S(I)$ had a considerably smaller staggering, see Fig. 6. It was thus concluded that one cannot expect vanishing staggering for chiral systems because the angles between the angular momenta are in general smaller than 90°. Furthermore, in principle vanishing energy staggering might be a consequence of a large moment-of-inertia and may not be related to possible chiral geometry of the angular momenta of the system.

Based on their investigations, Shirinda and Lawrie [6] concluded that both features of (i) specific staggering in the $B(M1)$ transition probabilities, and (ii) lack of energy staggering in the partner rotational bands, cannot be considered as reliable fingerprints of chiral symmetry. It was proposed to use calculations in order to evaluate the orientations of the angular momenta of the system and test whether chiral geometry is present.

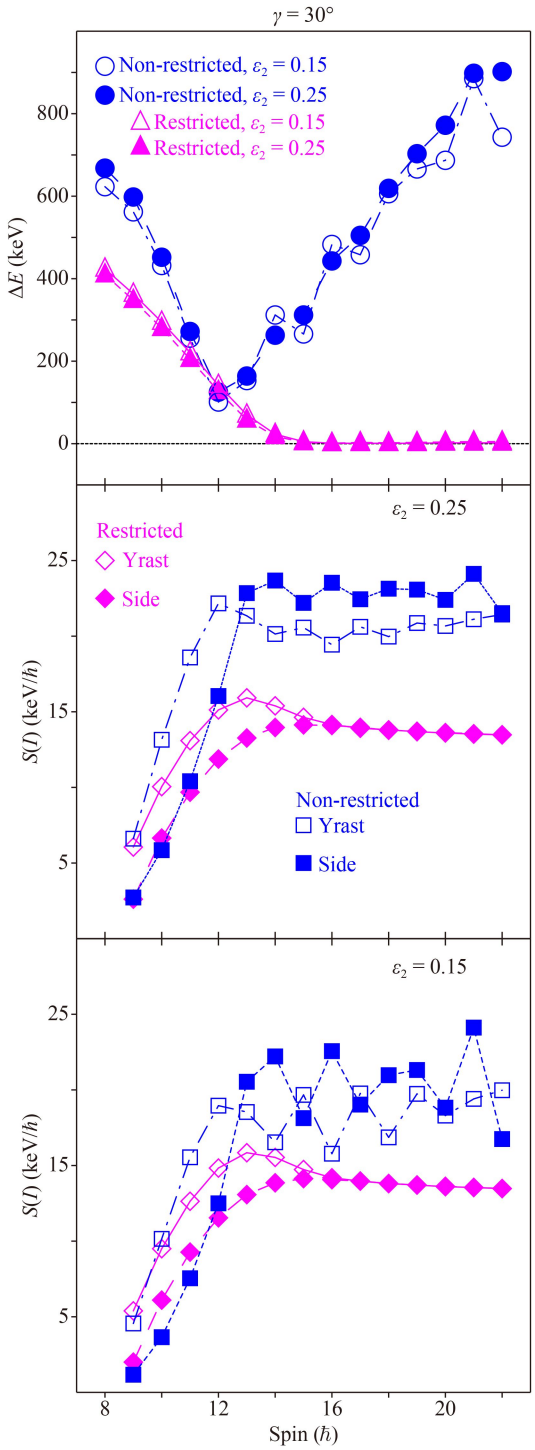

Fig. 6 Calculated energy staggering parameter $S(I) = [E(I) - E(I-1)]/(2I)$ and difference in the excitation energies ΔE of the $\pi h_{11/2} \otimes \nu h_{11/2}^{-1}$ partner bands for fixed single-particle angular momenta (restricted configuration space) and free single-particle angular momenta (non-restricted configuration space), at $\gamma = 30°$ and $\varepsilon_2 = 0.15$, 0.25. Reproduced from Ref. [6].

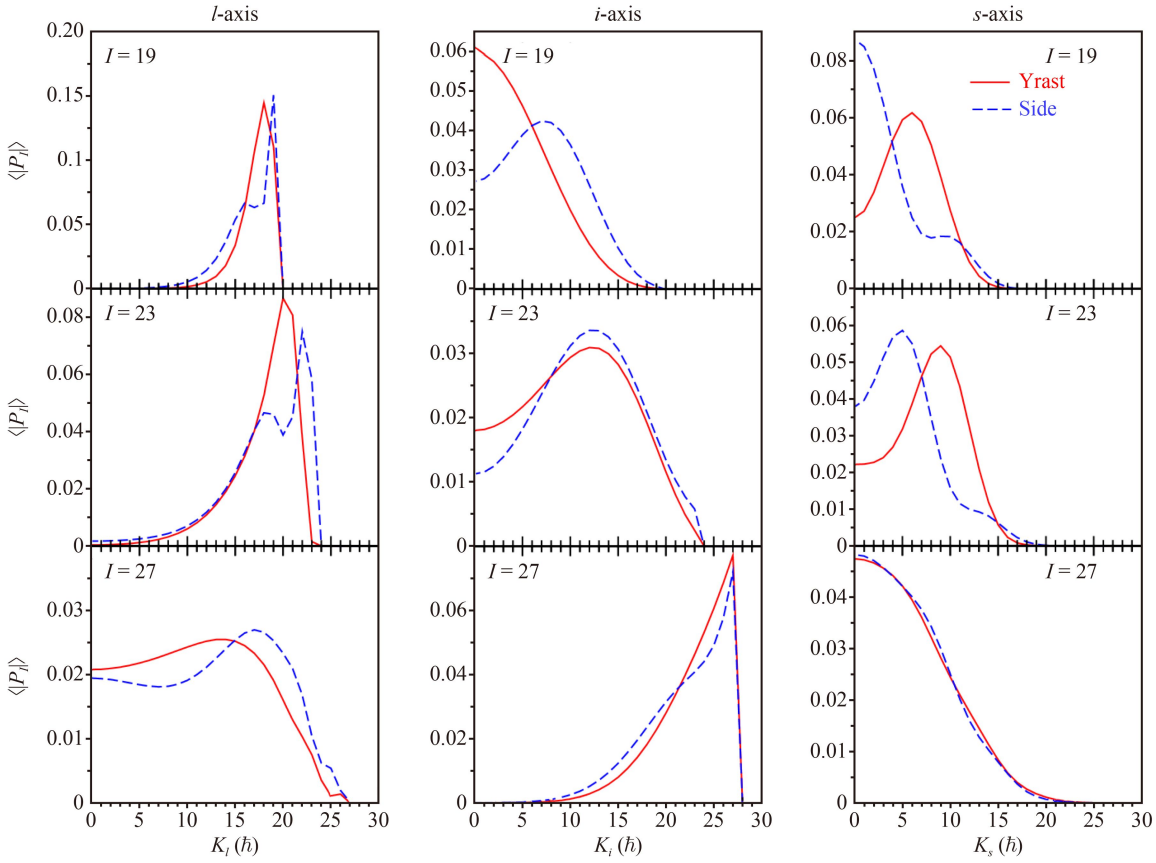

Fig. 7 Calculated probability distributions for the projections of the total angular momentum on the short (s), intermediate (i), and long (l) nuclear axes, for the yrast and the side $\pi h_{9/2} \otimes \nu i_{13/2}^{-3}$ partner bands and at $\gamma = 30°$ and $\varepsilon_2 = 0.15$. Reproduced from Ref. [11].

2.3 Asymmetric nucleon configurations

In order to form a chiral system one needs an aplanar orientation of the total angular momentum I. It may seem natural to assume that the best chiral geometry would form when I has similar projections on the three nuclear axes, that is j_π, j_ν, and R would have similar magnitudes. On the other hand several chiral partner bands with very good near-degeneracy (which would imply good chirality) were observed and associated with very asymmetric nucleon configurations, for instance with the three-quasiparticle $\pi h_{11/2}^2 \otimes \nu h_{11/2}^{-1}$ configuration in ^{135}Nd [9] and with the four-quasiparticle $\pi h_{9/2} \otimes \nu i_{13/2}^{-3}$ configuration in ^{194}Tl [10]. Therefore it was interesting to test whether chiral geometry could exist for very asymmetric nucleon configurations.

Shirinda *et al.* [11] used the Many-Particle Rotor Model [12], for the $\pi h_{9/2} \otimes \nu i_{13/2}^{-3}$ configuration, with $\varepsilon_2 = 0.15$, and $\gamma = 30°$. The probability distributions for the projections of the total angular momentum on the three nuclear axes are shown in Fig. 7. A peak at near-zero projection implies dominant planar components; however, when the distributions of all three projections of I peak at large, non-zero values, a chiral geometry is formed. Figure 7 shows that while near the band heads ($I \approx 19$) and at high spins ($I \approx 27$) planar components are indeed dominant, the states of both partner bands in the middle spin range ($I \approx 23$) have chiral geometry in angular momentum space. Therefore it was concluded that chiral geometry can also exist for strongly asymmetric nucleon configurations.

2.4 Many-particle chiral bands built on the same nucleon configuration

It was already shown in the seminal paper of Frauendorf and Meng [1], that a number of chiral systems can form with the same $\pi h_{11/2} \otimes \nu h_{11/2}^{-1}$ configuration. The yrast chiral system would be associated with the two lowest-energy bands, which become degenerate for spins above $I_c \sim 13\hbar$, see Fig. 1, while an excited chiral pair would comprise the next two bands that reach degeneracy near $I_c = 16\hbar$. In these calculations one can easily identify the bands that form the yrast (the two lowest-energy bands) and the excited (the third and fourth bands) chiral systems. However, in real nuclei where the single-particle angular momenta are not fixed to remain aligned along the short and long nuclear axes, the chiral

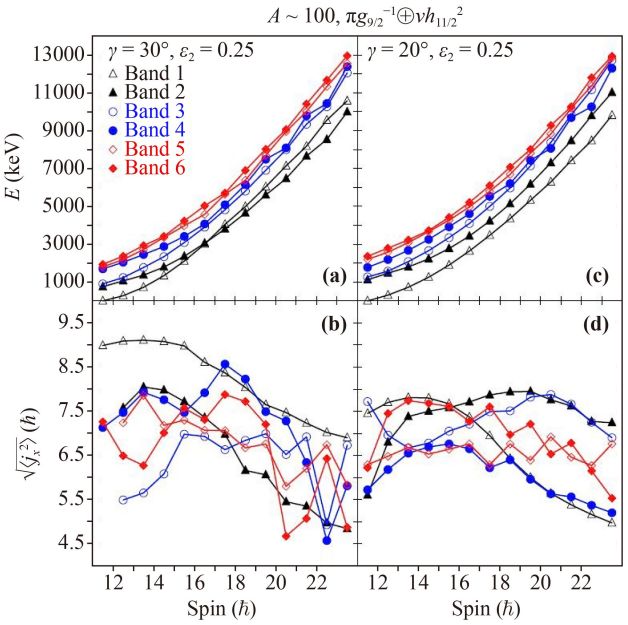

Fig. 8 Calculated excitation energies E and angular momenta of the neutrons j_n along the nuclear short x-axis for the six lowest-energy bands for realistic configuration descriptions and for the chiral bands at $\varepsilon_2 = 0.25$ and $\gamma = 20°, 30°$. The calculated bands are labelled bands 1, 2, 3, 4, 5 and 6 according to their excitation energy at low spin. Reproduced from Ref. [13].

partners show considerable differences in their excitation energies, and in some cases the bands may even cross each other. Thus, often it is not obvious how to group the observed bands into pairs of chiral partners. Shirinda and Lawrie studied such multiple chiral systems built on the same nucleon configurations in order to shed more light on such questions [13, 14].

Calculations were carried out for three typical three- and four-quasiparticle configurations relevant to the $A = 100$, 130, and 190 mass regions, respectively. The probability distributions of the projections of the total angular momenta suggested that chiral geometry is formed for all calculated cases. (For the $\pi g_{9/2}^{-1} \otimes \nu h_{11/2}^{2}$ configuration in the $A = 100$ mass region, see [14].)

The calculated excitation energies for the six lowest-energy $\pi g_{9/2}^{-1} \otimes \nu h_{11/2}^{2}$ bands in the $A = 100$ mass region are shown in Fig. 8 for $\gamma = 30°$ and 20°. One can group the bands into chiral pairs according to their excitation energies. In this case one would build the three chiral systems denoted on the figure with different colours. In order to study the similarity in the nature of such pairs the expectation values of the projections of the angular momenta for the neutrons along the short nuclear axis are also shown. It is clear that there is no specific similarity in the magnitudes and trends of these angular momenta for each pair of bands. For instance consider the calculations for $\gamma = 30°$. Bands 1 and 2, the bands that would naturally be associated with the yrast chiral system, show a large difference in their neutron angular momenta, as large as $\sim 2\hbar$. It could be noted that in fact the excited partner bands show closer similarity in these angular momenta, particularly Bands 5 and 6. The calculations for $\gamma = 20°$ again reveal distinctive differences in the magnitudes of these angular momenta for Bands 1 and 2. In this case at high spins there is a considerable similarity between the neutron angular momenta calculated for Bands 2 and 3, and for Bands 1 and 4, rather than for Bands 1 and 2. It was concluded that when searching for chiral bands it is best to find as many rotational bands with the same nucleon configuration as possible, and to evaluate their similarities including by testing their quasiparticle angular momenta [13, 14]. This may provide an important insight on the intrinsic nature of the bands. Very often the calculated partner bands for the yrast chiral system did not show particularly good near-degeneracy. By contrast, the similarity in the features in the excited chiral systems seemed considerably better. This suggests that excited chiral systems may possess better near-degeneracy and stronger chiral symmetry features.

As discussed above despite the numerous studies of chiral systems there are still no confirmed fingerprints that can be used for an unambiguous identification of chiral bands. An interesting idea, to study the decay patterns of rotational bands was suggested, in order to possibly exclude an alternative interpretation in terms of single-particle excitations, of the observed bands [15]. It was noted that a set of rotational bands that are built on different single-particle configuration (within the Cranked Shell Model notation) would follow a different decay pattern to that of a set of chiral partner bands [15]. Therefore one could carry out such studies, when applicable, to test and possibly rule out such an alternative interpretation.

3 Experimental techniques

3.1 Reactions

The study of chiral phenomena in atomic nuclei is essentially a study of how the nucleus can accommodate increasing angular momentum. Therefore, one of the best reactions for this purpose is the fusion-evaporation reaction [16], as the experimental study of chiral bands requires that relatively high-spin states of the nucleus be populated. Details of the various reactions used in the investigations are listed in Table 1. In general, heavier beams are desirable as the input angular momentum scales with the momentum of the beam. However, the choice of reaction is ultimately restricted by the available beam and target combinations that create the desired final nucleus. As the regions of interest for the study of nuclear chirality were often close to stability, lighter beams between ^{4}He and ^{18}O were often used to produce

Table 1 Details of experiments covered in this review.

Nucleus	Reaction(s)	Beam energy (MeV)	Target thickness (mg/cm^2)	Events ($\times 10^9$)	Refs.
Mass 80 region					
^{74}As	^{74}Ge(α,p3n)	59, 63	2.9 + backing	1.9 $\gamma\gamma$	Xiao, *et al.* [19]
^{78}Br	^{70}Zn(^{12}C,p3n)	60, 65	0.85	1.5 $\gamma\gamma$	Liu, *et al.* [20]
				0.16 p$\gamma\gamma$	Liu, *et al.* [20]
^{80}Br	^{76}Ge(^{11}B,α3n)	54	1.8 + backing	0.2 $\gamma\gamma$	Wang, *et al.* [21]
	^{76}Ge(^{7}Li,2n)	35	0.2, 0.6 + backing	1.2 $\gamma\gamma$ [a]	Wang, *et al.* [21]
^{81}Kr	^{82}Se (α,5n)	65, 68	0.4	1.5 $\gamma\gamma$	Mu, *et al.* [22]
^{82}Br	^{82}Se (α,p3n)	65, 68	0.4	1.5 $\gamma\gamma$	Liu, *et al.* [23]
Mass 100 region					
^{106}Ag	^{90}Zr (^{14}N,4n)	71	17	3.4 $\gamma\gamma$	Lieder, *et al.* [24]
			0.7	0.4 $\gamma\gamma$	Lieder, *et al.* [24]
Mass 190 region					
^{193}Tl	^{160}Gd(^{37}Cl,4n)	167	1.0		Ndayishimye, *et al.* [25]
	^{181}Ta(^{18}O,6n)	105	1.0	10.0 $\gamma\gamma$	Ndayishimye, *et al.* [25]
^{194}Tl	^{181}Ta(^{18}O,5n)	91, 93	Stacked 2 or 3 × 0.5	3.0 $\gamma\gamma$	Masiteng, *et al.* [10, 26]
	^{181}Ta(^{18}O,5n)	91	1.0 + backing	$\gamma\gamma$	Masiteng, *et al.* [27]
^{198}Tl	^{197}Au(α,3n)	40	13.0	$\gamma\gamma$	Lawrie, *et al.* [28, 29]
	^{197}Au(α,3n)	40	0.2	$e\gamma$ [b]	Lawrie, *et al.* [28, 29]

Note: [a] Data from Max-Planck-Institut fur Kernphysik Heidelberg [17].
[b] Orsay electron spectrometer [18].

the species of interest, limiting the angular momentum input to $\sim 20\hbar$.

The stable, heavy-ion beams at the iThemba LABS facility [30] are supplied by the Separated Sector Cyclotron. As this is a $k = 200$ cyclotron, proton beam energies of up to 200 MeV are available; for heavy-ions, the beam energy also depends on the charge state of the beam. At iThemba LABS, two Electron-Cyclotron Resonance Ion-sources (ECRIS) are available for charge breeding – ECRIS4, which was originally built by GANIL for the Helmholtz–Zentrum Berlin [31, 32] and GTS2, based on the design of the Grenoble Test Source [33]. The latter is able, for example, to produce useful ^{132}Xe beams in the 38^+ charge state, giving a beam energy of 2.2 GeV.

3.2 AFRODITE

Fusion-evaporation reactions leave the evaporation residues in high-spin states which decay chiefly by γ-ray emission. Thus γ-ray spectroscopy becomes the main tool for deciphering the properties of the excited states of the nucleus, including any chiral properties. The chief tool for γ-ray spectroscopy at iThemba LABS has been the AFRican Omnipurpose Detector for Innovative Techniques and Experiments (AFRODITE) [34, 35], an array of HPGe detectors. During the course of these investigations, which took place over a decade, AFRODITE would be configured with up to nine Compton-suppressed Clover [36–38] HPGe detectors, each with a peak-to-total ratio of up to 50%, and eight LEPS [34] HPGe detectors for a total photopeak efficiency of up to 1.6% at 1.3 MeV. The data acquisition system passed through various upgrades and is presently equipped with a digital data-acquisition system based on XIA LLC PIXIE-16 cards [39]. This system allows data to be taken in singles mode, which typically corresponded to a γ–γ coincidence event-rate of around 10 kHz.

The AFRODITE frame, that supports the detectors, can accommodate four Compton-suppressed clovers at 45° to the beam axis, eight at 90° and four at 135°. In a typical experiment, the clover detectors would be distributed equally around 90° and 135° to the beam axis. This geometry allows the formation of various ratios of Directional Correlations from Oriented (DCO) states [40], which assists in making spin-parity assignments. Data were recorded in coincidence mode, with the condition that a minimum of two γ-rays should be detected in separate detectors (doubles). A typical DCO ratio, R_{DCO}, between two γ-rays, $\gamma_1(\theta_i)$ and $\gamma_2(\theta_j)$ detected at angles $(\theta_{i,j}) = 135°$ or 90° was formed as

$$R_{DCO} = \frac{I(\gamma_1(90°)\gamma_2(135°))}{I(\gamma_1(135°)\gamma_2(90°))}. \quad (2)$$

If the first transition is of known stretched quadrupole character, typical R_{DCO} ratios give values close to 0.6, and 1, when the second transition is of stretched pure dipole or quadrupole character, respectively. Other values are possible depending on the value of the quadrupole–dipole mixing ratio of the second transition. An Angular Distribution from Oriented states (ADO) could also be formed as the ratio

$$R_{ADO} = \frac{I(\gamma(135°))}{I(\gamma(90°))}, \tag{3}$$

where the intensities $I(\gamma(\theta))$ are formed by summing over all coincidences of the type $I(\gamma_1(\theta)\gamma_2(\alpha))$, where $\alpha = 135°, 90°$. In the AFRODITE geometry, the R_{ADO} ratios are approximately 1.3 and 0.8 for stretched quadrupole and pure dipole transitions, respectively.

Further information on γ-ray multipolarities can be obtained with the AFRODITE array by measuring the linear polarisation $P(\theta)$ of the emitted γ-ray [41]. $P(\theta)$ is defined as the difference between γ-ray intensity with electric vector parallel to the reaction plane, (defined by the beam axis and the emitted γ-ray), and that with electric vector perpendicular to the reaction plane, normalised to their sum

$$P(\theta) = \frac{I(\theta, \phi = 0°) - I(\theta, \phi = 90°)}{I(\theta, \phi = 0°) + I(\theta, \phi = 90°)}. \tag{4}$$

The quantity $P(90°)$ is used to determine the electric or magnetic character of γ-ray transitions, as it is positive for both stretched $E1$ and $E2$ transitions, and negative for stretched $M1$ and $M2$ transitions. As the name suggests, the clover detectors have a four-fold segmentation formed by four distinct crystals, arranged in a "clover" pattern, which allows them to function as a Compton polarimeter [42]. Those clover detectors at $\theta = 90°$ are placed where $P(\theta)$ is a maximum. By measuring the intensity of γ-rays scattered from one crystal to the other, in a direction either parallel to the beam line $N_{//}$, or perpendicular to the beam line $N_{\perp}$, the linear polarisation anisotropy can be formed,

$$A_p = \frac{aN_{\perp} - N_{//}}{aN_{\perp} - N_{//}}, \tag{5}$$

where a represents the scattering efficiency of the detector. The linear polarisation and linear polarisation anisotropy are related through

$$A_p = Q(E_\gamma)P(\theta), \tag{6}$$

where Q is a measure of the efficiency of the polarimeter which depends on γ-ray energy. An internal calibration, using known transitions, can be made to determine $Q(E_\gamma)$.

The primary information determined by spectroscopy experiments are levels, spins and parities of nuclear states. More can be learned about the nature of excited states by measuring their lifetimes. These are related to nuclear transition matrix elements which in turn depend on the underlying nuclear structure of the nuclear states. Quantities such as in-band transition rates are a critical test of nuclear chirality, as they should be identical between the chiral partners. Level lifetimes have been measured with AFRODITE using the Doppler-Shift Attenuation Method (DSAM) method. This method exploits the fact that the energy of a γ-ray emitted from a nucleus is Doppler shifted, depending on the velocity, v, of the emitter and the angle of detection, θ, of the γ-ray:

$$E_\gamma = E_0\left(1 + \frac{v}{c}\cos\theta\right). \tag{7}$$

As the reaction product slows down in the target medium, the magnitude of the Doppler shift also decreases. A knowledge of the stopping power of the target medium for the reaction product allows the lifetime to be deduced. Since the Doppler shift is maximized at $\cos(\theta) = \pm 1$, experiments dedicated to DSAM measurements would have the detectors mounted at 45° and 135°. Examples of various lineshapes are given in Fig. 9. A 960.2 keV γ-ray de-excites a 10^- level in ^{106}Ag, and because the 10^- state decays after the nucleus has stopped, the 960.2 keV line shows only the instrumental resolution. By contrast, the 966.6 keV line shows a Doppler-shifted tail on the high-energy side of the peak at 45°, and a low-energy tail at 135°, corresponding to decays of a 16^- state while the nucleus slowed down in the target.

The line shape would be simulated using a software package such as the system COMPA, GAMMA, SHAPE [43–45]. This package would use Monte Carlo methods

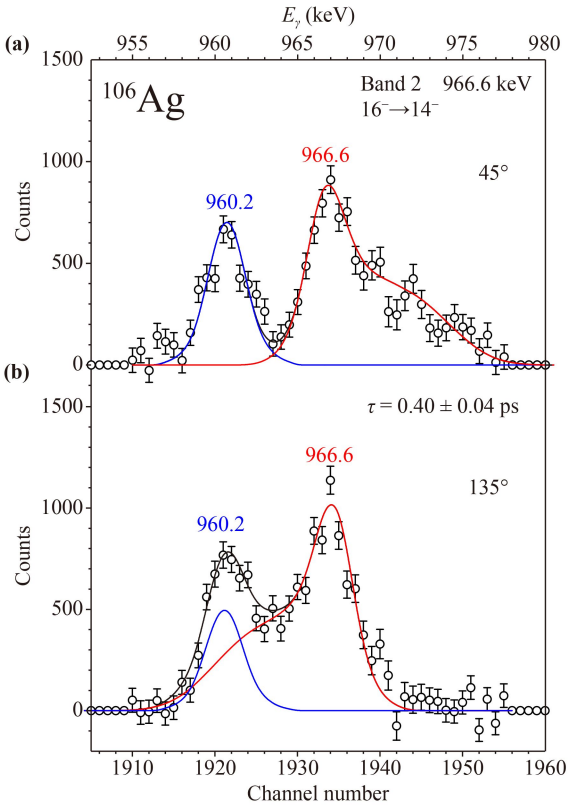

Fig. 9 An example of a DSAM line-shape analysis [24]. The 966.6 keV γ-ray line is the transition that deexcites the 16^- level of Band 2 in ^{106}Ag. **(a)** The 45° spectrum (forward direction) and **(b)** the 135° spectrum (backward direction).

to simulate all processes contributing to the lineshape, including the stopping down process of the nucleus in the target material, and the population and decay of all states on the path feeding the level of interest. The latter required calculation of the fusion-evaporation process, consideration of statistical $E1$, $M1$ and $E2$ transitions and cascades of $E2$ and $M1$ transitions. The nuclear properties required as input for such calculations were taken from the parameters in the literature [46, 47]. Examples of the quality of the fitted lineshapes are given by the solid lines shown in Fig. 9.

3.3 DIAMANT

Higher sensitivity of the AFRODITE array can be achieved by coupling it to an ancillary device that is able to select the reaction of interest and thereby reject unwanted background events. As many of the reactions listed in Table 1 involve the emission of charged particles, the charged particle array DIAMANT [48, 49] was often employed to enhance the selectivity of AFRODITE. DIAMANT is an array of 54 CsI(Tl) scintillators, each 3 mm thick and approximately 1 cm^2 in area, covering a total of 95% of 4π. As momentum considerations favour the emission of particles into the forward direction, the "Chessboard" [50] comprising a 4×4 array of DIAMANT CsI(Tl) scintillators, was also employed at 0°, depending on availability.

4 New regions of chirality

As we have seen above, the conditions required for the manifestation of strict chirality in atomic nuclei are rather demanding. The basic requirement is the existence of a triaxial nucleus, followed by the requirement for large particle angular-momentum components to be aligned with the long and short axes of the triaxial nucleus. In the seminal paper on chirality, Frauendorf and Meng [1] identified the mass 130 region as prospective for nuclear chirality. They suggested the level scheme of ^{134}Pr as presenting possible experimental evidence of a chiral pair, in which the particle angular momenta were supplied by an $h_{11/2}$ proton particle on the short axis and an $h_{11/2}$ neutron hole on the long axis. While measurements of transition probabilities [51, 52] in ^{134}Pr later excluded this as a case of nuclear chirality, it prompted a search for other candidates in the region [53, 54], with the case of ^{128}Cs emerging as the best example of nuclear chirality [55].

In the mass 100 region, the next region of chirality to be explored, the $\pi g_{9/2}^{-1} \otimes \nu h_{11/2}$ configuration would supply the particle angular momenta in ^{104}Rh [8]. Going lighter still, to the mass 80 region, chirality would be associated with the $\pi g_{9/2} \otimes \nu g_{9/2}$ configuration. In a heavier prospective region of chirality, with mass around 190, chiral bands could be formed from $h_{9/2}$ proton particles and $i_{13/2}$ neutron holes, to form the $\pi h_{9/2} \otimes \nu i_{13/2}^{-1}$ configuration. Both these new regions of chirality, with mass 80 and mass 190, were discovered at iThemba LABS.

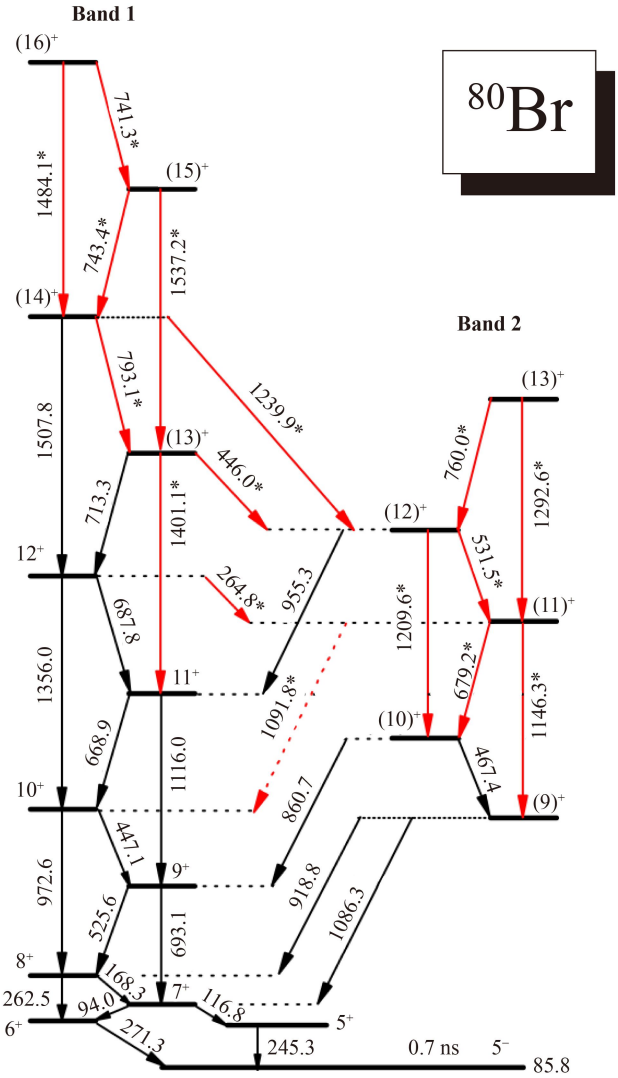

Fig. 10 Partial level scheme of ^{80}Br showing the chiral partners Band 1 and Band 2. Transitions added by Wang *et al.* [21] are indicated by stars and red lines.

4.1 Mass 80 region

The first candidate for chirality in the mass 80 region was ^{80}Br. The partial level scheme shown in Fig. 10 is the result of two experiments, one at iThemba LABS, utilising AFRODITE and the Chessboard, and the other experiment, at Max-Planck-Institut für Kernphysik Heidelberg [17], employing six EUROBALL CLUSTER detectors. Wang *et al.* [21] added a completely new band to the level scheme – Band 2 – and used a DCO analysis to deduce that it has the same parity as Band 1, which

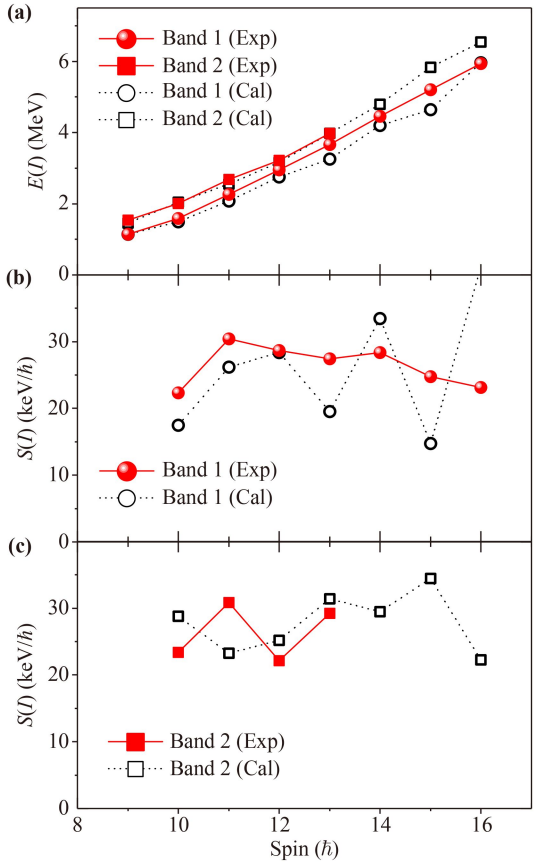

Fig. 11 **(a)** Excitation energy and **(b)**, **(c)** staggering parameter $S(I) = [E(I) - E(I-1)]/(2I)$ as a function of spin for the doublet bands in ^{80}Br. The filled (open) symbols connected by solid (dotted) curves denote experimental (theoretical) values [21].

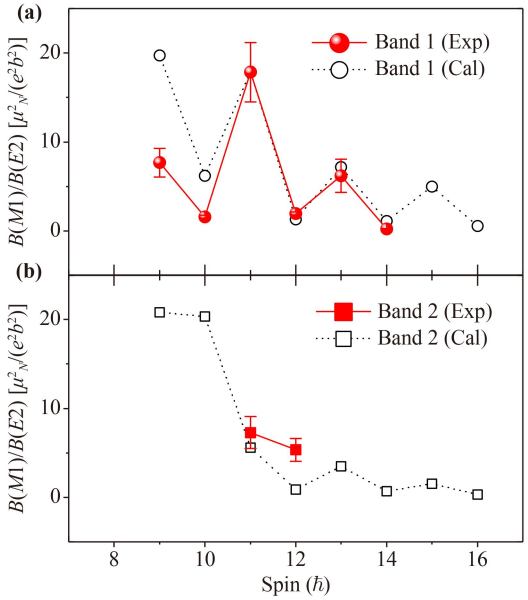

Fig. 12 Comparisons of the measured and calculated in-band $B(M1)/B(E2)$ ratios for the bands 1 **(a)** and 2 **(b)** in ^{80}Br [21].

had been assigned [56] to the $\pi g_{9/2} \otimes \nu g_{9/2}$ configuration. The fact that Band 2 was too low in energy to be a γ-vibration coupled to Band 1, taken together with the existence of numerous interband $E2$ and $M1/E2$ transitions, suggested Band 2 as a possible chiral partner to Band 1. The interpretation of the character of Bands 1 and 2 was made with the assistance of Relativistic Mean Field (RMF) Theory [57], which formed the basis for input into the Triaxial Particle Rotor Model (TPRM) [58] calculations. According to the RMF, the deformation of the nucleus in the $\pi g_{9/2} \otimes \nu g_{9/2}$ configuration is triaxial, with $\beta_2 = 0.346$ and $\gamma = 24.59°$. This deformation implies lifetimes of the lowest-spin members of Band 1 that are in good agreement with measurements [56]. The resulting TPRM calculations are compared with experiment in Figs. 11 and 12. Although the main features of the level energies and staggering parameter $S(I)$ of the bands are reproduced (Fig. 11), an overestimate of $S(I)$ is seen which is likely caused by a lack of Coriolis attenuation in the calculations [21].

By contrast, the in-band $B(M1; I \to I-1)/B(E2; I \to I-2)$ values plotted in Fig. 12 show a good agreement between experiment and theory. However, the same calculations showed that the angular momentum of the hole-like $g_{9/2}$ valence neutron had a large mixture of components with projections on both the long and intermediate axes, departing from the picture of ideal chiral geometry. The calculated probability distributions for the projection of the total angular momentum along the l-, i- and s-axes are given in Fig. 13. They differ for the two bands at the bandhead ($I = 9\hbar$), with that of Band 1 being maximum at $K_i = 0\hbar$ and Band 2 being maximum at $K_i = 6\hbar$, indicating an oscillation of the collective angular momentum through the s–l-plane. Therefore, Wang *et al.* [21] concluded that the bands in ^{80}Br were consistent with a chiral vibration, rather than static chirality, which would require identical K distributions.

The discovery of chirality in the mass 80 region stimulated the Shandong group to an intense experimental programme at iThemba LABS to search for more examples in the region. The level scheme of ^{82}Br, deduced by Liu *et al.* [23] is shown in Fig. 14. Bands 1 and 2 were identified as chiral partners using similar criteria as for ^{80}Br – an examination of level energies, staggering $S(I)$, and $B(M1)/B(E2)$ values, which were all in satisfactory agreement with the TPRM. Unlike ^{80}Br, for which the TPRM calculations were consistent with a chiral vibration, the calculated angular momentum probability distributions for the two bands, along the various axes, shown in Fig. 15, are approximately equal in the spin interval of 9 to 12$\hbar$, implying that in this interval, ^{82}Br could be interpreted as exhibiting static chirality.

Other nuclei to be studied in this mass region include ^{74}As, ^{78}Br and ^{81}Kr, as listed in Table 1. New phenomena

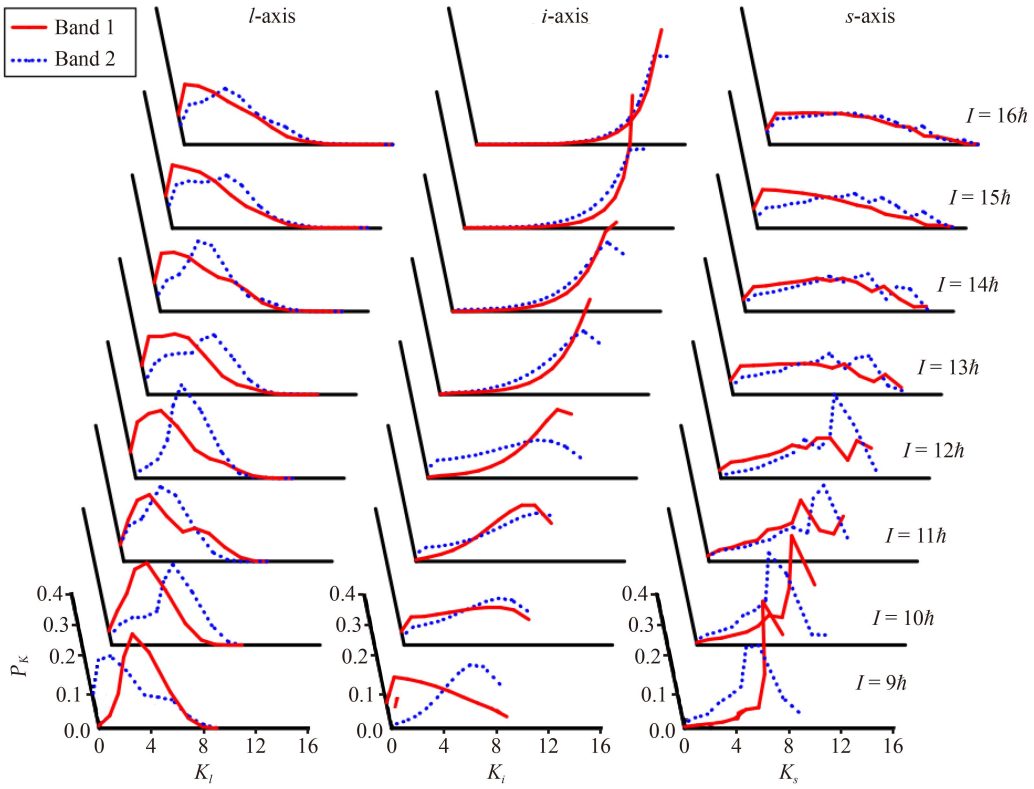

Fig. 13 The probability distributions for projection of total angular momentum on the long (l-), intermediate (i-) and short (s-) axis in TPRM for the doublet bands in ^{80}Br [21].

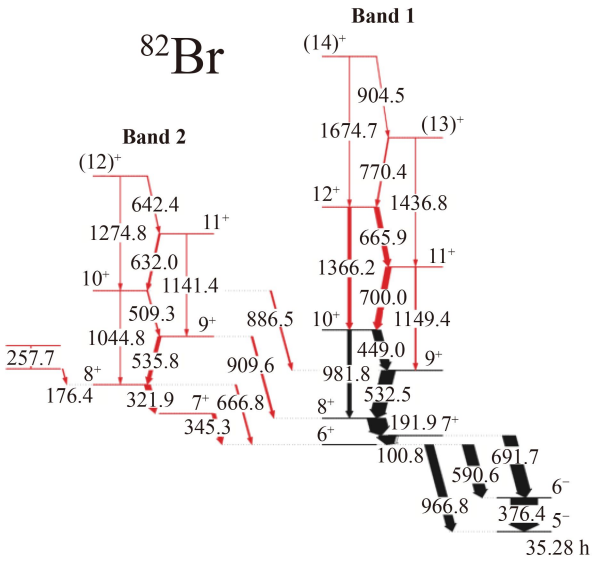

Fig. 14 Partial level scheme of ^{82}Br showing the chiral partners Band 1 and Band 2. New transitions and levels are indicated in red [23].

such as the existence of octupole correlations between chiral bands in ^{78}Br and ^{74}As, and the observation of peudo-spin triplet bands in ^{81}Kr were observed. These discoveries are discussed in detail in Section 7 below.

4.2 Mass 190 region

The ^{198}Tl nucleus was the first case of nuclear chirality to be identified in the Tl isotopes in the mass 190 region [28, 29]. The Tl isotopes are the only mass region where chirality is associated with nuclei with triaxial deformation with $\gamma > 30°$.

Lawrie *et al.* [28, 29] observed a chiral pair in ^{198}Tl, shown in the partial level scheme of Fig. 16, using data from experiments with the AFRODITE array at iThemba LABS, and the electron spectrometer at Orsay [18], as detailed in Table 1. The yrast band had been assigned by Kreiner *et al.* [71] to the $\pi h_{9/2} \otimes \nu i^{-1}_{13/2}$ configuration – a configuration with angular momentum components on the short and long axes of the nucleus. The level scheme was extended by adding a new side-band, and confirming a low-energy 71.8 keV transition at the head of the yrast band, implying a signature inversion in the band. The combination of ADO, polarization and conversion coefficient measurements allowed firm spin assignments to be made to the yrast band and its partner. The new side band was associated with the same $\pi h_{9/2} \otimes \nu i^{-1}_{13/2}$ configuration, as no other two-quasi-particle configuration involving orbitals close to the proton and neutron Fermi levels in ^{198}Tl could provide the observed high spin and negative parity [28]. In addition, the observed alignments, moments-of-inertia and

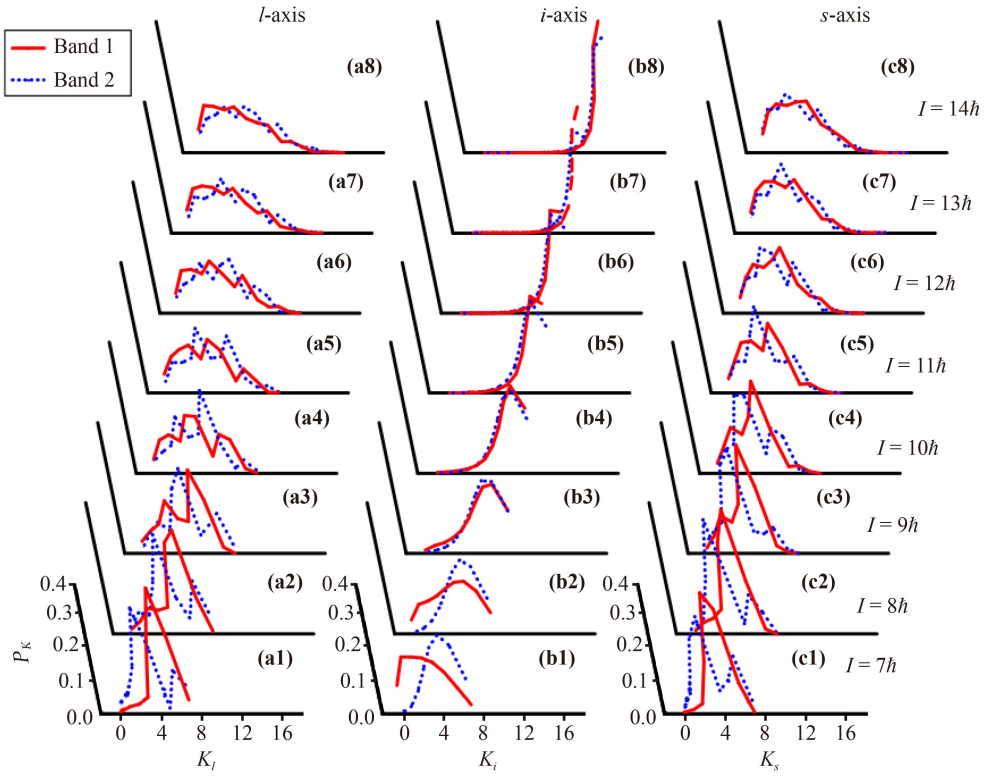

Fig. 15 The probability distributions for projection of total angular momentum on the long (l-), intermediate (i-) and short (s-) axis in TPRM for the doublet bands in ^{82}Br [23].

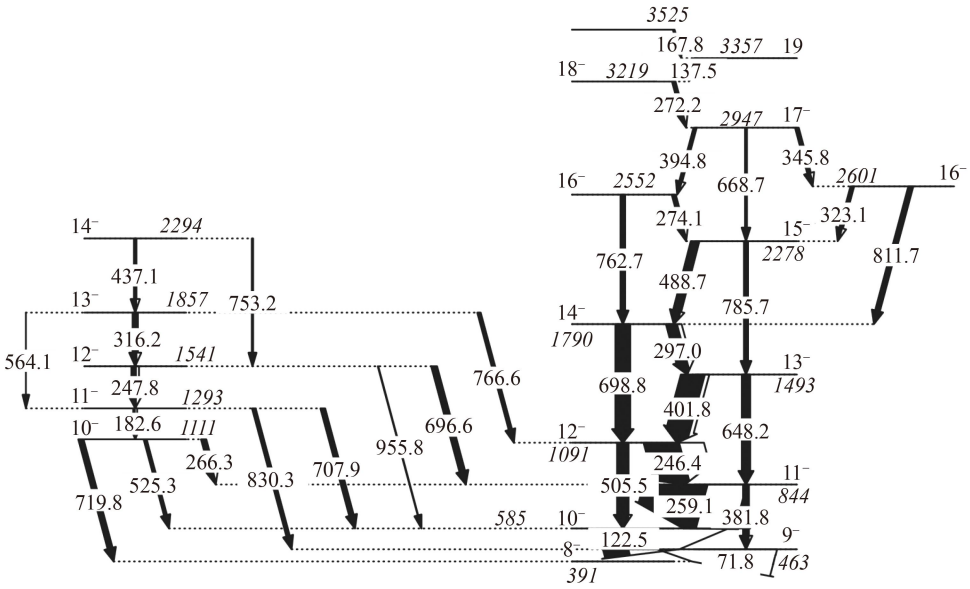

Fig. 16 Partial level scheme [28] showing the pair of chiral bands in ^{198}Tl.

$B(M1)/B(E2)$ ratios were found to be almost identical for both $\pi h_{9/2} \otimes \nu i_{13/2}^{-1}$ bands, in line with expectations for a chiral pair with perfect mutual orthogonality of the three angular momenta. On the other hand, the excitation energies differ by ~ 500 keV and considerable energy staggering is observed in the yrast band. As discussed in Sections 2.1 and 2.2 above, such features are not surprising for real chiral partner bands [3, 6]. In order to study whether these bands correspond to a chiral system, the triaxiality of the nuclear shape of ^{198}Tl was investigated using two-quasiparticle-plus-triaxial-rotor model (QTR) calculations.

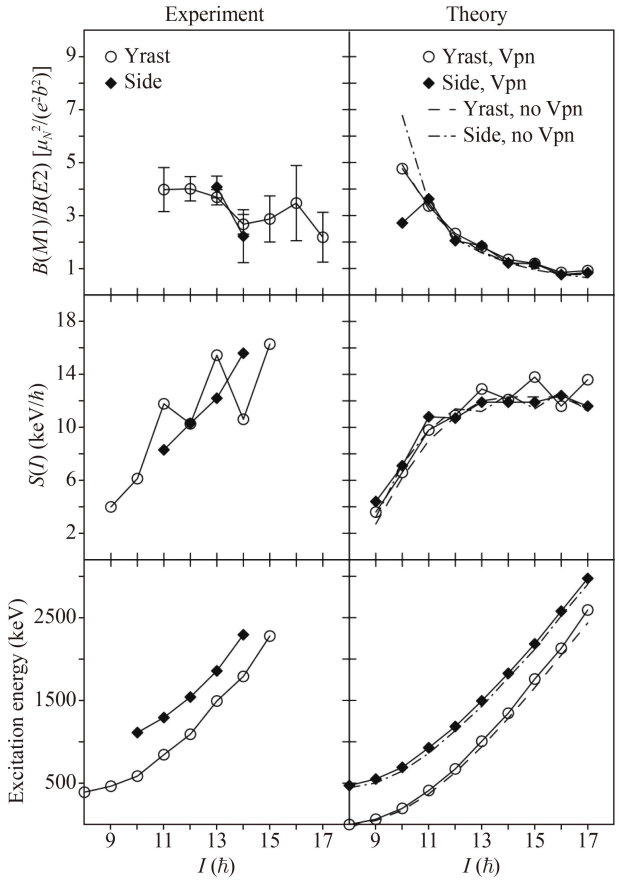

Fig. 17 Experimental (left panels) and calculated (right panels) excitation energies, staggering $S(I) = [E(I) - E(I-1)]/(2I)$, and $B(M1)/B(E2)$ transition probability ratios for the yrast and side bands in ^{198}Tl at $\gamma = 44°$. The calculations with and without proton–neutron (V_{pn}) interaction are shown. Reproduced from Ref. [29].

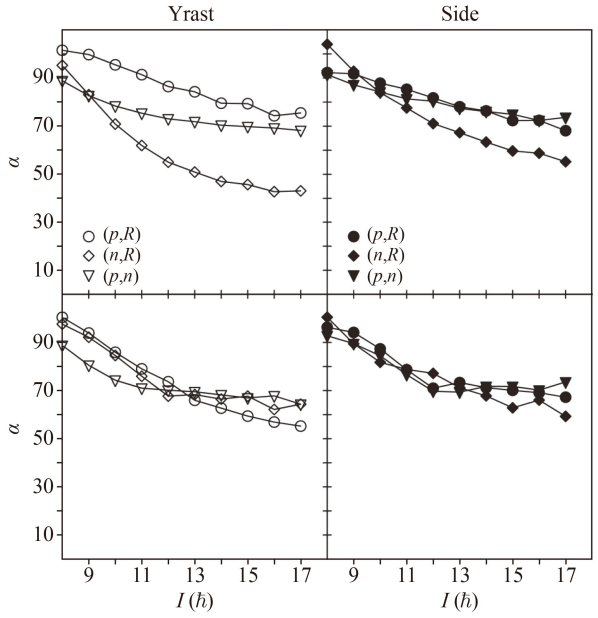

Fig. 18 Calculated average angles between the angular momentum of the collective rotation and those of the proton $\alpha(p,R)$ and neutron $\alpha(n,R)$ and also the angle between the angular momenta of the proton and neutron $\alpha(p,n)$ for $\gamma = 44°$ (top panels) and $\gamma = 30°$ (bottom panels), and for the yrast and side bands in ^{198}Tl [29].

It is known that in order to form a chiral system, a triaxial nuclear shape would be required to contribute angular momentum along the intermediate axis. The even-even neighbours of ^{198}Tl had been previously associated with triaxial shapes with $\gamma \sim 36°$ [59–61]. To determine the magnitude of the triaxial deformation in ^{198}Tl, Lawrie *et al.* [28] compared the experimental data for the $\pi h_{9/2} \otimes \nu i^{-1}_{13/2}$ pair of bands with QTR [4, 5] calculations for different γ deformations. As the $\pi h_{9/2} \otimes \nu i_{13/2}$ bands exhibit signature inversion that can be explained in the QTR model with the inclusion of a residual proton–neutron interaction [62, 63], the residual interaction

$$V_{pn} = \sqrt{8\pi^3}\left(\frac{\hbar}{m\omega}\right)^{3/2} \delta(\boldsymbol{r}_p - \boldsymbol{r}_n)(u_0 + u_1 \sigma_p.\sigma_n) \quad (8)$$

was included, where the parameters u_0 and u_1 were set to previously determined values [63].

The calculations were in best agreement with the experimental data for triaxial deformation of $\gamma = 44°$, [28]. As shown in Fig. 15, the calculations reproduce (i) the magnitude and the almost constant relative excitation energy of the two bands as a function of spin, (ii) the observed signature staggering in the yrast band and its lack in the side band, and (iii) the smooth trend and the equal values of the $B(M1)/B(E2)$ ratios for both bands. The importance of using calculations with proton–neutron (V_{pn}) interaction, particularly when the calculations are intended to describe the energy staggering of the bands, is worth noting. Indeed, the same calculations but without V_{pn}, fail to reproduce the experimental energy staggering in these bands.

In order to examine whether chiral geometry was formed, the expectation values of the projections of the angular momenta of the valence proton, neutron and rotation along the nuclear axes were calculated. It was found that these angular momenta were predominantly aligned along the short, long and intermediate axes, respectively, supporting a chiral geometry [28]. In addition, the calculated expectation values for the angles between these angular momenta were found to be close to 90°, near the bands heads for the two bands, and decreasing at higher spins, but remaining larger than 40° up to highest spins, see Fig. 18 [29]. These results suggest that the three angular momenta indeed form a chiral geometry.

Lawrie *et al.* [29] also studied the orientation of the angular momenta of the valence proton and neutron. The probability distributions of the projections of these

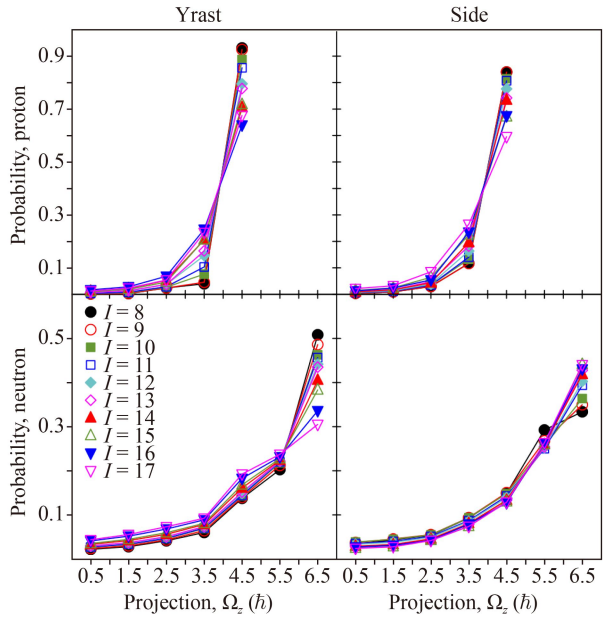

Fig. 19 Calculated distributions of the projections of the angular momenta of the proton and neutron along the short and long axes, respectively, for $\gamma = 44°$ and for the yrast and side bands in ^{198}Tl [29].

two angular momenta along the short and long nuclear axes, respectively, are shown in Fig. 19. As the angular momenta of the valence proton and neutron are not fixed along the short and long nuclear axes, respectively, contributions with different projections also appear, in particular at higher spins. Nevertheless, the contribution with largest alignment of $4.5\hbar$ along the short axis for the proton and of $6.5\hbar$ along the long axis for the neutron remain largest for both bands and for all spins, confirming that these angular momenta are predominantly aligned along these two axes. Such orientation, when coupled with the dominant orientation of the rotation along the intermediate axis, confirmed further that an aplanar orientation of the total angular momentum was formed.

5 Close near-degeneracy and multiple bands

Following the discovery of a chiral system in the $A = 190$ mass region [28], other Tl isotopes were investigated at iThemba LABS. Experiments with the AFRODITE array revealed new chiral systems also in the ^{193,194}Tl isotopes. The chiral system in ^{193}Tl is associated with the $\pi h_{9/2} \otimes \nu i_{13/2}^{-2}$ configuration [25]. In ^{194}Tl two chiral systems were observed, based on the $\pi h_{9/2} \otimes \nu i_{13/2}^{-1}$ and $\pi h_{9/2} \otimes \nu i_{13/2}^{-3}$ configurations [10]. This is the only known case where the chiral geometry of the angular momenta in the two-quasiparticle chiral pair persists through a band crossing and into a four-quasiparticle configuration. Most importantly, the observed $\pi h_{9/2} \otimes \nu i_{13/2}^{-3}$ pair revealed a very close near-degeneracy between the chiral partners, one of the best known to date [10].

5.1 ^{194}Tl

The analysis of the experiments on ^{194}Tl with the AFRODITE array (for details see Table 1) allowed Masiteng *et al.* [10, 26] to expand the previously known $\pi h_{9/2} \otimes \nu i_{13/2}^{-1}$ band [64] and to observe a new partner band built on the same nucleon configuration, see Bands 1 and 4 shown in the partial level scheme in Fig. 20. Both partner bands were extended through a band crossing and into a $\pi h_{9/2} \otimes \nu i_{13/2}^{-3}$ four-quasiparticle configuration. A number of linking transitions between the bands both below and above the band crossings supported the proposed configuration assignments.

The excellent near-degeneracy of the observed chiral partner bands with four-quasiparticle configuration was highlighted [10]. These partner bands have similar excitation energies; with energy difference not more than 110 keV throughout the whole spin range of the bands and reaching a minimum value of 37 keV for the states with $I = 21$, see Fig. 21. In addition, the four-quasiparticle bands show practically identical alignments [65], i_x, and similar $B(M1)/B(E2)$ transition probability ratios. These features were compared with the features of some good chiral partners, such as the two-quasiparticle bands in ^{128}Cs [66], ^{104}Rh [8] and the three-quasiparticle band in ^{135}Nd [9, 67] and found that the pair in ^{194}Tl represents one of the best near-degeneracies, thus one of the best nuclear chiral symmetry cases observed to date [10].

Masiteng *et al.* [10] also evaluated the expected triaxiality of the nuclear shape for these bands of ^{194}Tl using the Cranked Nilsson–Strutinsky (CNS) codes [12, 68], see Fig. 22. The deepest energy minimum was found to have a moderately deformed quadrupole deformation with $\varepsilon_2 = 0.17$ and $\gamma = -43°$ at $I = 11$, and to persist to high spins, ($I = 21$). The triaxial deformation implies favored rotation along the intermediate axis. Coupling the rotational angular momentum along the intermediate axis with the quasiparticle angular momenta of the proton along the short axis and of the neutron(s) along the long axis would generate chiral geometry in angular momentum.

In addition to the chiral pair, details about another negative-parity band, denoted as Band 3 in Fig. 20 were also reported [26]. This band was associated with the same $\pi h_{9/2} \otimes \nu i_{13/2}^{-3}$ configuration as the four-quasiparticle chiral partners Bands 1 and 4. It was the first time a competition between a chiral pair and another band built on the same configuration was observed.

It was noted that while the energies of the four-quasiparticle chiral pair are very similar, Band 3 has somewhat lower excitation energy, see Fig. 23 [25, 26]. Also while the alignments of the chiral partner bands are almost

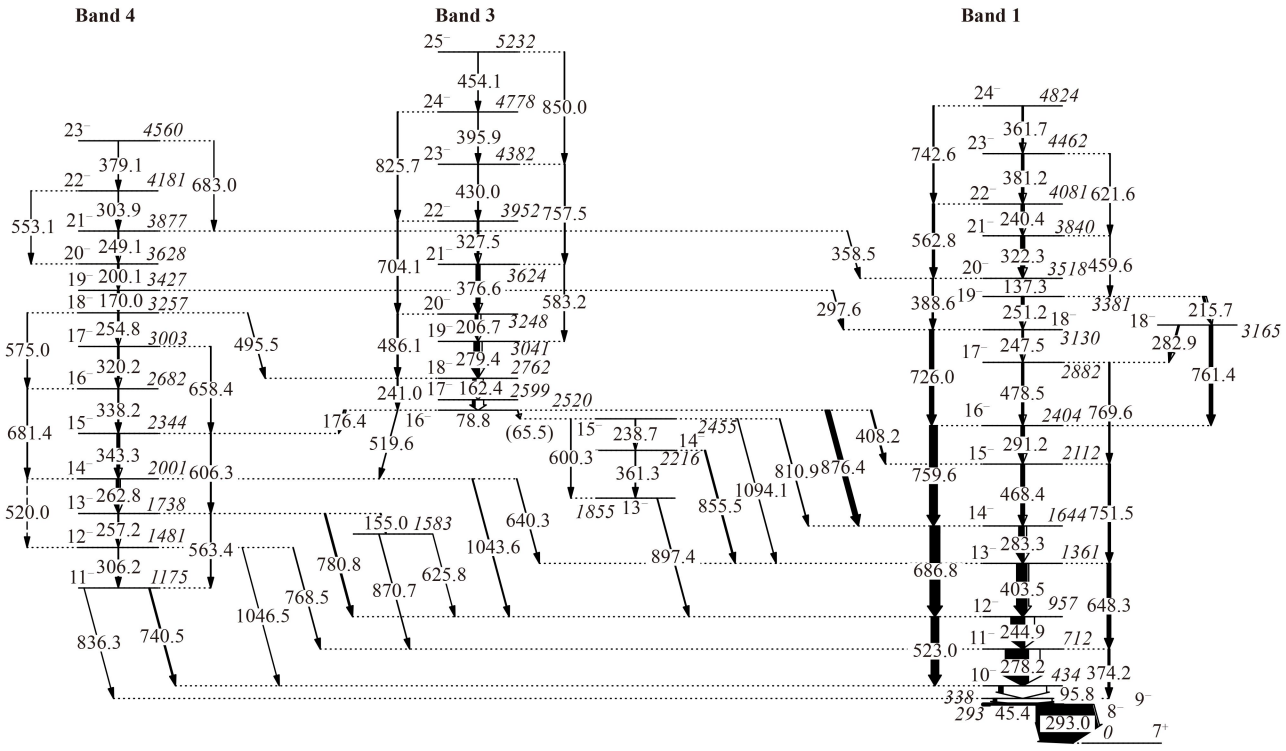

Fig. 20 Partial level scheme showing the negative-parity bands in ^{194}Tl. The yrast and the side bands from the chiral pair are denoted as Bands 1 and 4, respectively [26].

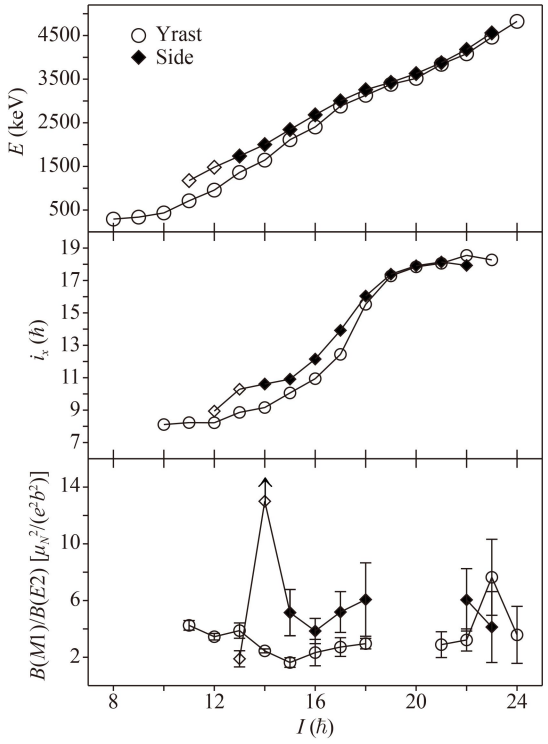

Fig. 21 Excitation energies, alignments, and $B(M1)/B(E2)$ ratios for the partner bands in ^{194}Tl. Data involving the 11^- and 12^- levels of the side band are shown with open diamonds. The alignments are calculated with reference parameters of $\Im_0 = 8\hbar^2$ MeV^{-1} and $\Im_1 = 40\,\hbar^4$ MeV^{-3}. Reproduced from Ref. [10].

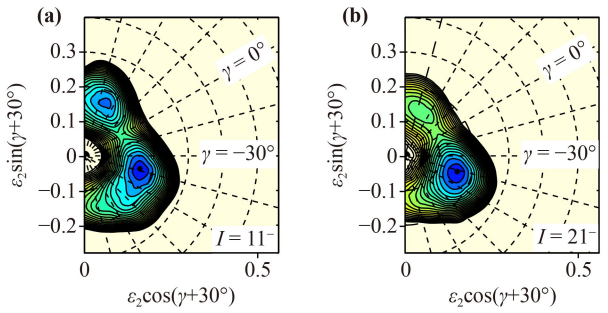

Fig. 22 Potential energy as a function of deformation for the negative parity bands in ^{194}Tl at **(a)** $I = 11^-$ and **(b)** $I = 21^-$. The spacing between the contour lines is 0.25 MeV. Reproduced from Ref. [10].

identical, the alignment of Band 3 is lower by (1.5–2) $\hbar$, as shown in Fig. 24. The alignment of the chiral pair was found to correspond well to the alignment expected by the additivity rule, where the alignments of the odd proton (in the $\pi h_{9/2}$ band in ^{193}Tl) is added to the alignment of the $\nu i_{13/2}^{-3}$ band in the ^{193}Hg isotone, see the red dashed line in Fig. 23. Thus while the chiral pair corresponds to a full alignment of the $\pi h_{9/2} \otimes \nu i_{13/2}^{-3}$ configuration, Band 3 has an incomplete alignment.

For the triaxial shape suggested by the CNS calculations, see Fig. 22, more than one chiral pair built on the same configuration may form. Thus in addition to the chiral partners (Bands 1 and 4) it is possible to see

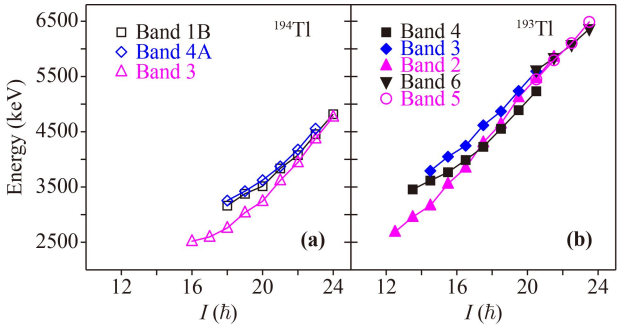

Fig. 23 Excitation energies for the $\pi h_{9/2} \otimes \nu i_{13/2}^{-n}$, where $n =$ 2,3 bands in ^{194}Tl **(a)** and in ^{193}Tl **(b)**. Reproduced from Ref. [26].

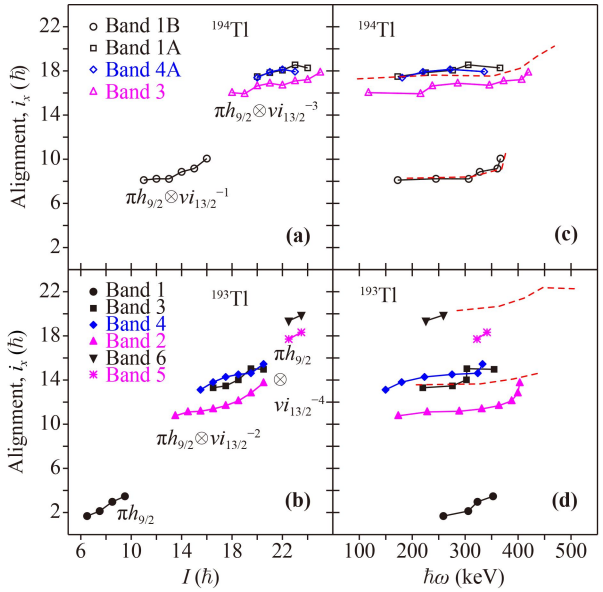

Fig. 24 Alignments for the $\pi h_{9/2} \otimes \nu i_{13}^{-n}$ bands, where $n =$ 0,1,2,3,4 in ^{193,194}Tl as a function of the initial spin I in panels **(a)** and **(b)**, and as a function of the rotational frequency in panels **(c)** and **(d)**. Harris parameters of $\Im_0 = 8\hbar^2$ MeV^{-1} and $\Im_1 = 40\hbar^4$ MeV^{-3} were used. The red dashed line in panels (c) and (d) indicates the experimental alignment of the corresponding $\nu i_{13/2}^{-n}$ band in the Hg isotone increased by 2.1 $\hbar$, a value that corresponds to the approximate alignment of the $h_{9/2}$ proton. Reproduced from Ref. [26].

another chiral pair comprising for instance Band 3 and another (yet unobserved) band. If the chiral partner of Band 3 is lying at similar (or higher) excitation energy than those of Bands 1 and 4, it might remain unobserved. Alternatively, it was argued that there could be a competition between rotational bands corresponding to triaxial (the chiral pair of Bands 1 and 4) and axially symmetric (Band 3) nuclear shapes [26]. However, no sign of axially symmetric shapes was observable on the potential energy surfaces shown in Fig. 22.

In order to study further the nature of the negative-parity bands in ^{194}Tl, Masiteng *et al.* [27] carried out DSAM lifetime measurements with the AFRODITE array. Details about the experiment are listed in Table 1. An example of the line shape analysis is shown in Fig. 25, while the derived lifetimes are given in Fig. 26.

The experimentally measured $B(M1)$ and $B(E2)$ transition probabilities for the three negative-parity bands in ^{194}Tl are shown in Fig. 27. It is clear that these experimental values are similar (within the experimental uncertainties) for all three negative-parity bands. Thus there is no sign of a difference in the nucleon configuration or in the nuclear shape corresponding to these bands.

Masiteng *et al.* [27] studied the expected features of the rotational bands built on the $\pi h_{9/2} \otimes \nu i_{13/2}^{-3}$ configuration, using theoretical calculations with the MPR model [12]. A triaxial shape with $\varepsilon_2 = 0.15$ and $\gamma = 30°$ and 40° was adopted. The calculated orientation of the angular momenta supported chiral geometry for all four calculated bands, denoted in Fig. 27 as A, B, C, and D. For $\gamma = 30°$ the calculated excitation energies of these bands indicated two well defined chiral pairs, where the yrast chiral pair comprises bands A and B, while the excited pair is built of bands C and D. This grouping is based on the observed gap between the excitation energies of these two pairs at high spins. However, as discussed above, see Section 2.1, the near-degeneracy in the calculated yrast chiral pair is in many case not as close as that of the excited chiral pairs. The differences are particularly large for $\gamma \neq 30°$ and asymmetric configurations. In the present case, for $\gamma = 40°$, the side band in the yrast chiral pair lies at energies similar to those of the bands in the excited chiral pair and this relative placement looks very similar to the experimental observation. Thus while all four calculated bands correspond to chiral geometry, it becomes unclear how to group them into chiral pairs.

It was also noted that the calculated $B(M1)$ and $B(E2)$ transition probabilities for the chiral bands with $\pi h_{9/2} \otimes \nu i_{13/2}^{-3}$ configuration are similar to each other and in agreement with the experimentally measured values [27]. It was thus considered that all three observed $\pi h_{9/2} \otimes \nu i_{13/2}^{-3}$ bands in ^{194}Tl could correspond to triaxial shape and have chiral geometry. Within this interpretation a fourth band with the same configuration would be expected at similar excitation energy as Bands 3 and 4. Such a band was not observed experimentally; however, its possible presence could not be ruled out [27].

5.2 ^{193}Tl

Following the observation of three competing rotational bands with possibly chiral nature in ^{194}Tl, Ndayishimye *et al.* [25] investigated the neighbouring ^{193}Tl. The excited states were studied with the AFRODITE array, for details on the experiment see Table 1. Modifications and an extension of the previously reported [69] level scheme of ^{193}Tl were proposed, see the partial level

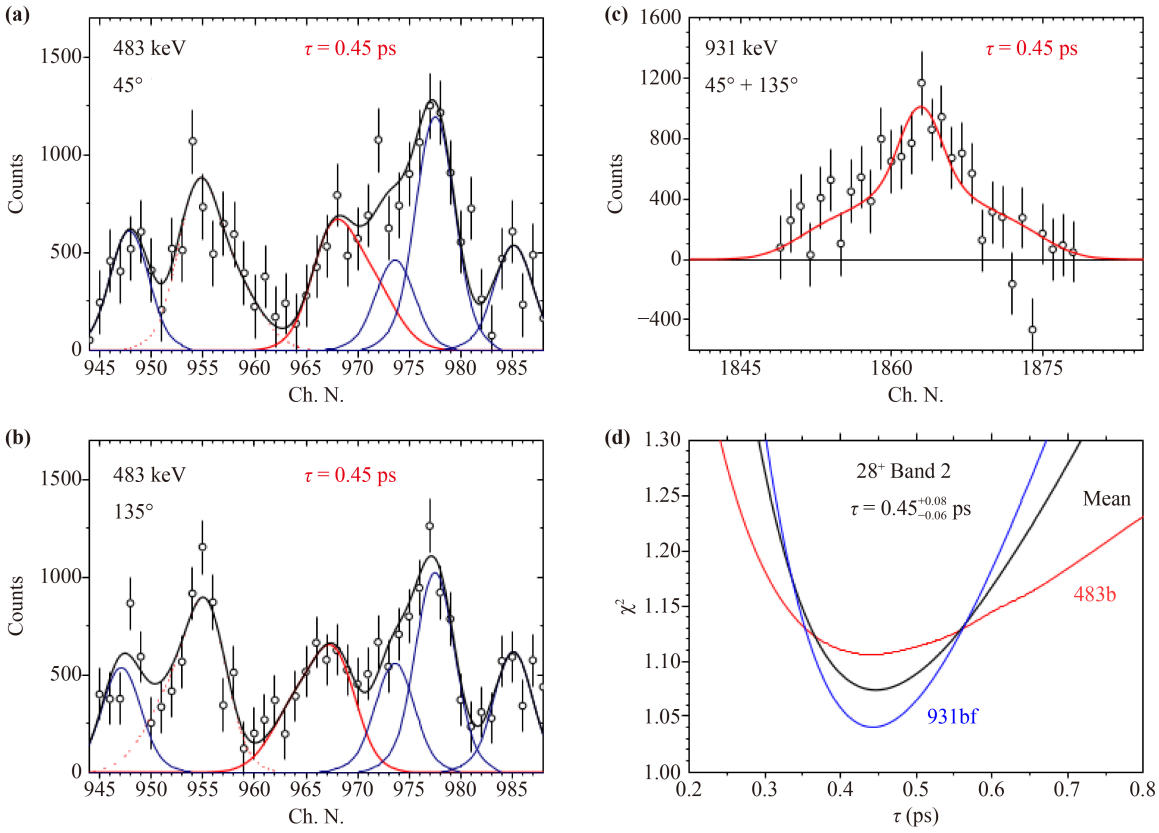

Fig. 25 Line shape analysis of two transitions de-exciting the 28^+ level of Band 2. Analysis of the 483-keV peak at **(a)** forward and **(b)** backward, angles, and **(c)** analysis of the 931-keV peak in the spectrum that is a sum of the forward and backward spectra. The fit of the Doppler broadened peak of interest is shown with red solid line. Peaks without Doppler broadening are fitted with apparatus line shapes, shown in blue. The black solid line shows the fit for all peaks. In panel **(d)** the χ^2 functions from the analysis of the spectra shown in (b) and (c) are plotted. Reproduced from Ref. [27].

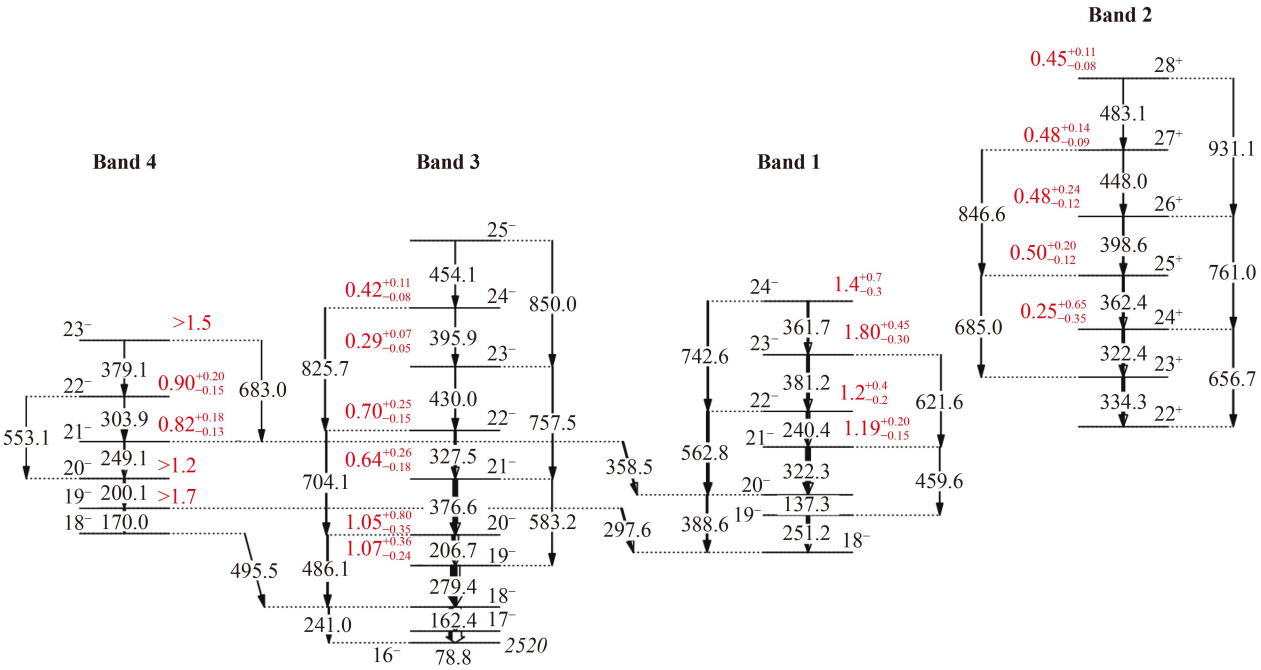

Fig. 26 Partial level scheme of the high-energy part of four bands of ^{194}Tl. The lifetimes (shown in red) are measured in ps. Reproduced from Ref. [27].

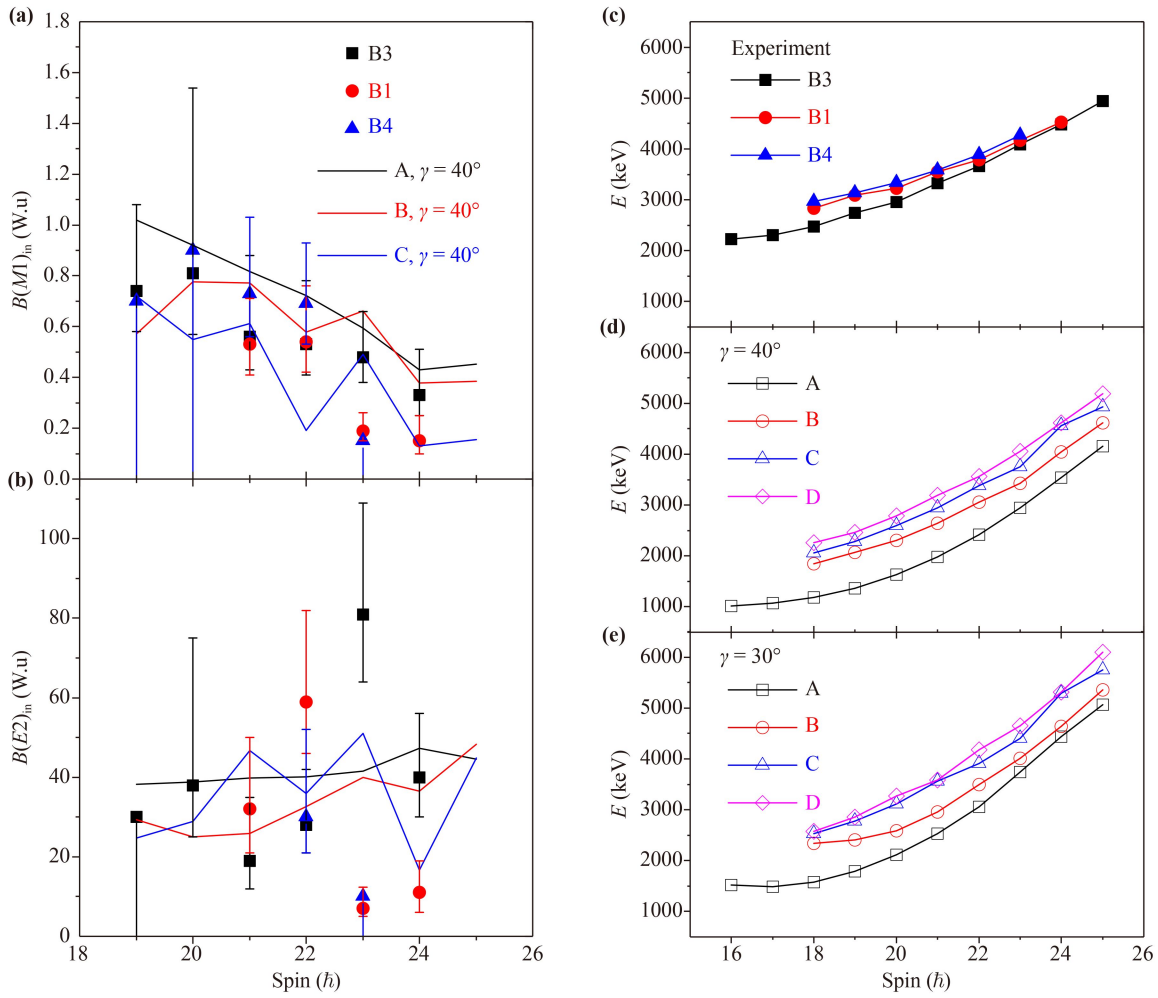

Fig. 27 Experimental and calculated **(a)** $B(M1)$, and **(b)** $B(E2)$, transition probabilities in the negative-parity bands of ^{194}Tl. Measured excitation energies are shown in **(c)**. The calculated energies for the four lowest-energy bands and for $\gamma = 40°$ and $\gamma = 30°$ are plotted in **(d)** and **(e)**, respectively. The calculated bands are labeled with A, B, C and D according to their excitation energy. Reproduced from Ref. [27].

scheme, shown in Fig. 28. The yrast $\pi h_{9/2} \otimes \nu i_{13/2}^{-2}$ band was modified near its band head, and Bands 3 and 4 were revised and extended. Two new five-quasiparticle bands, Bands 5 and 6, were also reported.

The three observed $\pi h_{9/2} \otimes \nu i_{13/2}^{-2}$ bands in ^{193}Tl were compared with the three $\pi h_{9/2} \otimes \nu i_{13/2}^{-3}$ bands in ^{194}Tl. The excitation energies and the alignments of these bands are shown in Figs. 23 and 24. As in ^{194}Tl, one of the bands in ^{193}Tl lies at lower excitation energy. Like the bands in ^{193}Tl, the yrast band has a smaller alignment than that for the two excited bands, which matches the expected full alignment of the valence nucleons, shown with dashed red lines in Fig. 24. Therefore it is very likely that the observed bands in ^{193,194}Tl have similar nature.

The CNS energy surfaces for ^{193}Tl at $I = 14.5$ and 18.5 are shown in Fig. 29. The deepest energy minimum is found for $\gamma = -45°$ which corresponds to a triaxial shape and a rotation around the intermediate axis. It suggests chiral orientation of the angular momenta and the presence of chiral partner bands.

Figure 29 also shows a second, shallower energy minimum at $\gamma = -90°$. This minimum also corresponds to triaxial nuclear shape but the rotation is around the long nuclear axis. It does not support chiral systems because the total angular momentum is oriented in the plane of the short and long nuclear axes.

Additional Cranked Shell Model (CSM) calculations were carried out to evaluate the expected $\nu i_{13/2}^{-2}$ alignments for nuclear shapes with $\gamma = -45°$ and with $\gamma = -90°$. It was found that for the former case the alignment of the two $i_{13/2}$ neutrons (corresponding to Routhians A, and B) is largest, while for $\gamma = -90°$ the A Routhian is shifted to higher energy and the two lowest energy Routhians, B and C, correspond to lower alignment. Therefore according to these calculations the expected alignment of two $i_{13/2}$ neutrons will be larger for $\gamma = -45°$ (for the chiral pair) than for $\gamma = -90°$ (for the single band). Such

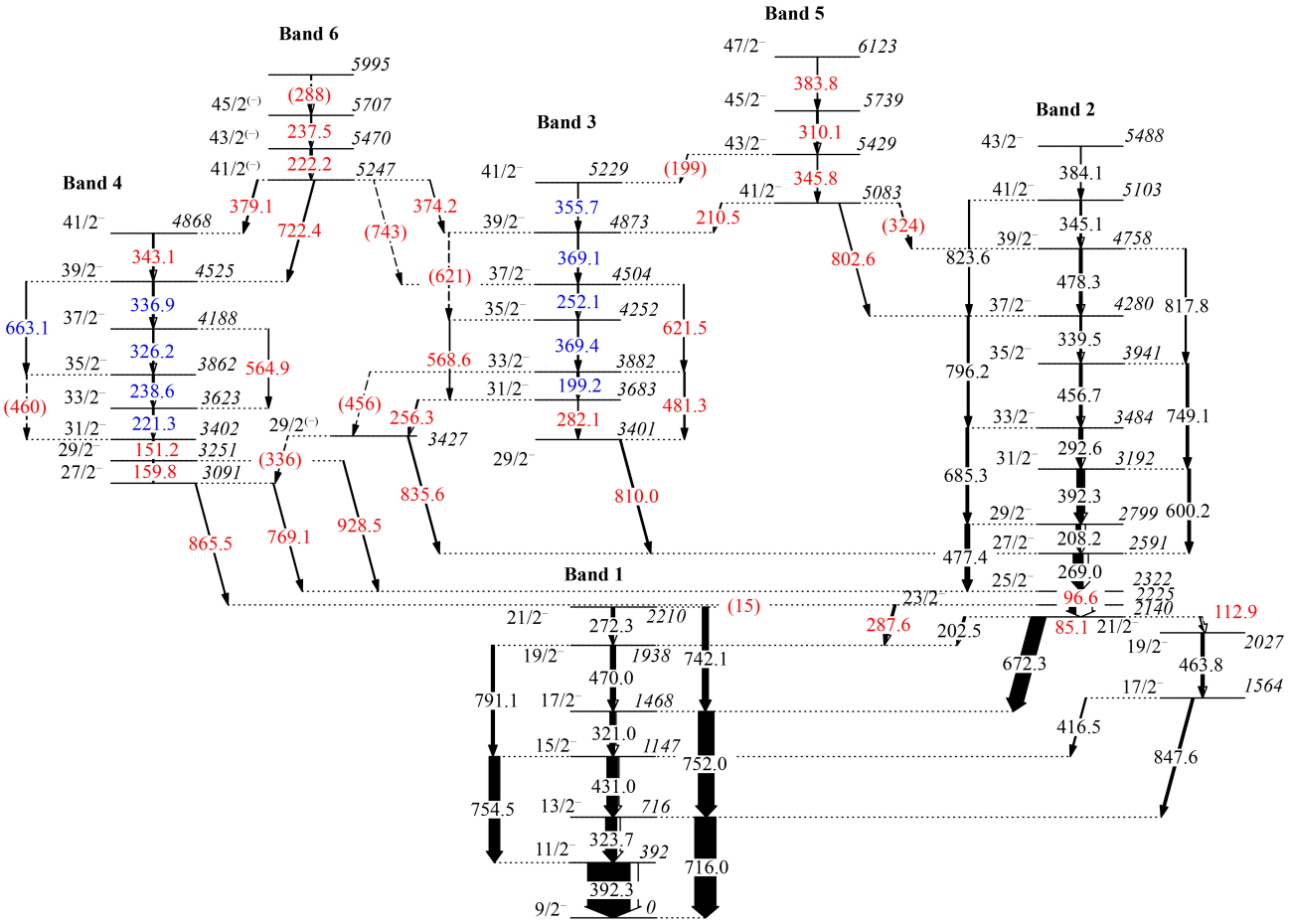

Fig. 28 Partial level scheme of ^{193}Tl. New transitions are shown in red. Transitions with revised placement are shown in blue. Reproduced from Ref. [25].

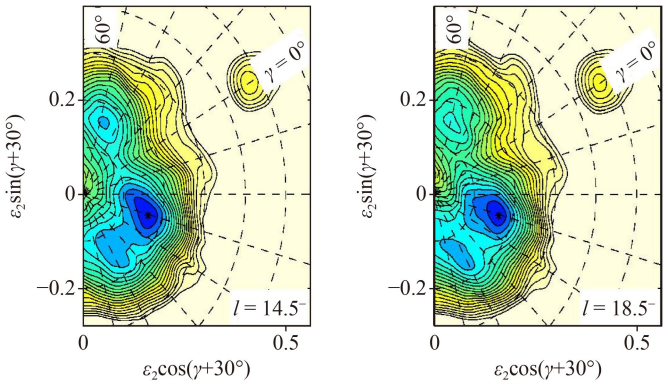

Fig. 29 Potential energy surfaces calculated with the cranked Nilsson–Strutinsky codes for the negative-parity bands in ^{193}Tl. Reproduced from Ref. [25].

difference in the alignments is in agreement with the experimental data.

Thus, two possible interpretations can be considered for the observed negative-parity bands in ^{193,194}Tl. The first was proposed initially for the $\pi h_{9/2} \otimes \nu i_{13/2}^{-3}$ bands in ^{194}Tl [27]. It is based on the assumption that all three of the observed bands correspond to nuclear shape with $\gamma \sim -40°$. Within this scenario all three bands have chiral geometry of the angular momenta. It implies that two chiral systems are generated, the yrast one corresponding to the $\nu i_{13/2}$ orbitals closest to the Fermi level, with the largest alignments, while the excited one corresponds to $\nu i_{13/2}$ orbitals with lower alignment. This scenario predicts four rotational bands, one at lower energy, while the other three bands lie at higher (and similar to each other) excitation energies. The shortcomings of this description are that (i) only three rotational bands have been observed to date, and (ii) contrary to these calculations the observed lowest-energy band has lower alignment that the excited bands.

The second interpretation assumes a competition between rotational bands associated with $\gamma \sim -45°$ and with $\gamma \sim -90°$. The former would correspond to chiral geometry of the angular momenta and produce a chiral pair. The latter would have a planar orientation of the total angular momentum and produce a single band. Therefore three rotational bands are expected within this scenario, in agreement with the experimental observations. In addition, according to the CSM results the

alignment for the chiral pair would be larger than that of the single band. The shortcomings of this interpretation are that the CNS calculations find a deeper energy minimum at –45° than at –90°, indicating that the chiral pair should have lower excitation energy than the single band. In addition, while a secondary energy minimum was found at $\gamma = -90°$ in ^{193}Tl, see Fig. 29, no sign of similar energy minimum was noticed for ^{194}Tl, see Fig. 22.

Ndayishimye *et al.* [25] considered that the second interpretation, in terms of competing rotations around the intermediate and long nuclear axes, was more probable for ^{193}Tl, although the first one, in terms of multiple chiral systems built on the same configuration, could not be ruled out. More detailed studies on the Tl isotopes would be very useful to shed more light on the nature of these competing negative-parity bands.

6 Resolution of a chiral conundrum in the mass 100 region

Early calculations [1, 54] of chiral pairs predicted that the transition from planar to aplanar rotation – the onset of static chirality – would be accompanied by the crossing of the yrast chiral partner by the yrare partner, after which the two bands would remain approximately degenerate until high spins, when the core angular momentum would dominate and return the nucleus to principal axis rotation. Indeed the first candidate chiral pair, in the nucleus ^{134}Pr, exhibited such a crossing near spin $14\hbar$, with the pair of bands continuing close in energy to spin $19\hbar$ [70]. In the nucleus ^{134}La, an extrapolation of the yrare band implied a crossing, but it was not extended to sufficient spin to be confirmed [54], while in the isotones of ^{134}Pr, ^{130}Cs, ^{132}La, and ^{134}Pm, the yrare partner never crossed the yrast partner, instead running approximately parallel.

It remained until a new region of chirality was explored, the mass 100 region, before another potential example of a crossing between yrare and yrast chiral candidates would be reported. In the nucleus ^{106}Ag, the $\pi g_{9/2}^{-1} \otimes \nu h_{11/2}$ configuration was involved in a crossing [72]. However, rather than interpret the bands as a pair of chiral partners, Joshi *et al.* [72] suggested that the yrast band of the nucleus corresponded to a triaxial shape, while its excited partner band was explained in terms of an axial nuclear shape. Shape transformation induced by chiral vibration was given as possible explanation for a planar axial rotational band being a partner of a triaxial band [72].

To come to a deeper understanding of the nature of the bands in ^{106}Ag, the nucleus was studied at iThemba LABS by Lieder *et al.* [24] using the AFRODITE array, in experiments detailed in Table 1. Two different targets were used; a thin one allowed the reaction products to recoil into vacuum so that γ-rays would be emitted with minimal Doppler broadening, thereby enabling transitions from high-spin states to be easily observed. A thicker target was used for a DSAM measurement of lifetimes of levels in the vicinity of the crossing region.

A partial level scheme deduced in this work [24] is shown in Fig. 30. It shows three negative-parity bands, where Bands 1 and 2, which cross near spin $14\hbar$, are the bands assigned to the $\pi g_{9/2}^{-1} \otimes \nu h_{11/2}$ configuration, as discussed by Joshi *et al.* [72], and where Band 3 is included because it could potentially play a role in chiral phenomena. Not shown is a fourth band of positive parity, which had been assigned to the $\pi g_{9/2}^{-1} \otimes \nu \{d_{5/2} g_{7/2}\} \nu h_{11/2}^2$ configuration [73].

An example of the DSAM analysis is given for the 966.6 keV transition of Band 2 in Fig. 9. It shows the fitted lineshape (red line), comprising a shifted and unshifted component in the forward and backward angles (45°, 135°). The lifetimes obtained from the DSAM experiment, accurate to 20%, are given on the level scheme (Fig. 30). These, along with branching ratios, were used to obtain $B(M1)/B(E2)$ ratios and absolute $B(M1)$ and $B(E2)$ values, as shown in Fig. 31.

In Fig. 32, quasiparticle alignments, i, are shown for Bands 1 to 3. There is a difference of nearly $4\hbar$ in aligned angular momentum between Bands 1 and 2, ruling out a simple interpretation in terms of chiral partners, which led to Joshi *et al.* [72] to suggest that the difference was due to planar and aplanar rotations. However, the approach taken by Lieder *et al.* [24] was to exploit the additivity of quasiparticle alignments to perform an empirical analysis. Aligned angular momenta, obtained by fitting alignments in neighbouring odd-particle nuclei, were added together to predict the aligned angular momenta for various configurations in ^{106}Ag. These are shown as solid lines in Fig. 32. A good agreement is obtained for Band 1, with the $\pi g_{9/2}^{-1} \otimes \nu h_{11/2}$ configuration. The quasiparticle alignments of Bands 2 and 3 are too low to be identified with the suggestion [74] of a $\pi g_{9/2}^{-1} \otimes \nu h_{11/2}^3$ configuration, but rather are in good agreement with the predicted aligned angular momenta for the (mixed) $\pi g_{9/2}^{-1} \otimes \nu \{g_{7/2}, d_{5/2}\}^2 h_{11/2}$ configuration. These assignments were further supported by RMF [75–79] calculations which confirmed that the empirically assigned configurations would lie lowest, with prolate deformations near $\beta = 0.2$ for Bands 1 to 3. The alignments, calculated using the RMF, shown in Fig. 32, are in good agreement with experiment. The quasiparticle alignment was also calculated for $\gamma = 30°$ but such a value could not reproduce the data. Finally the TPRM was used to calculate the experimental energies and transitions shown in Fig. 31. The satisfactory agreement between experiment and theory led to the conclusion that the bands could not be identified as chiral bands, but rather, were of two and four quasiparticle nature. The second possible example of a pair of crossing chiral

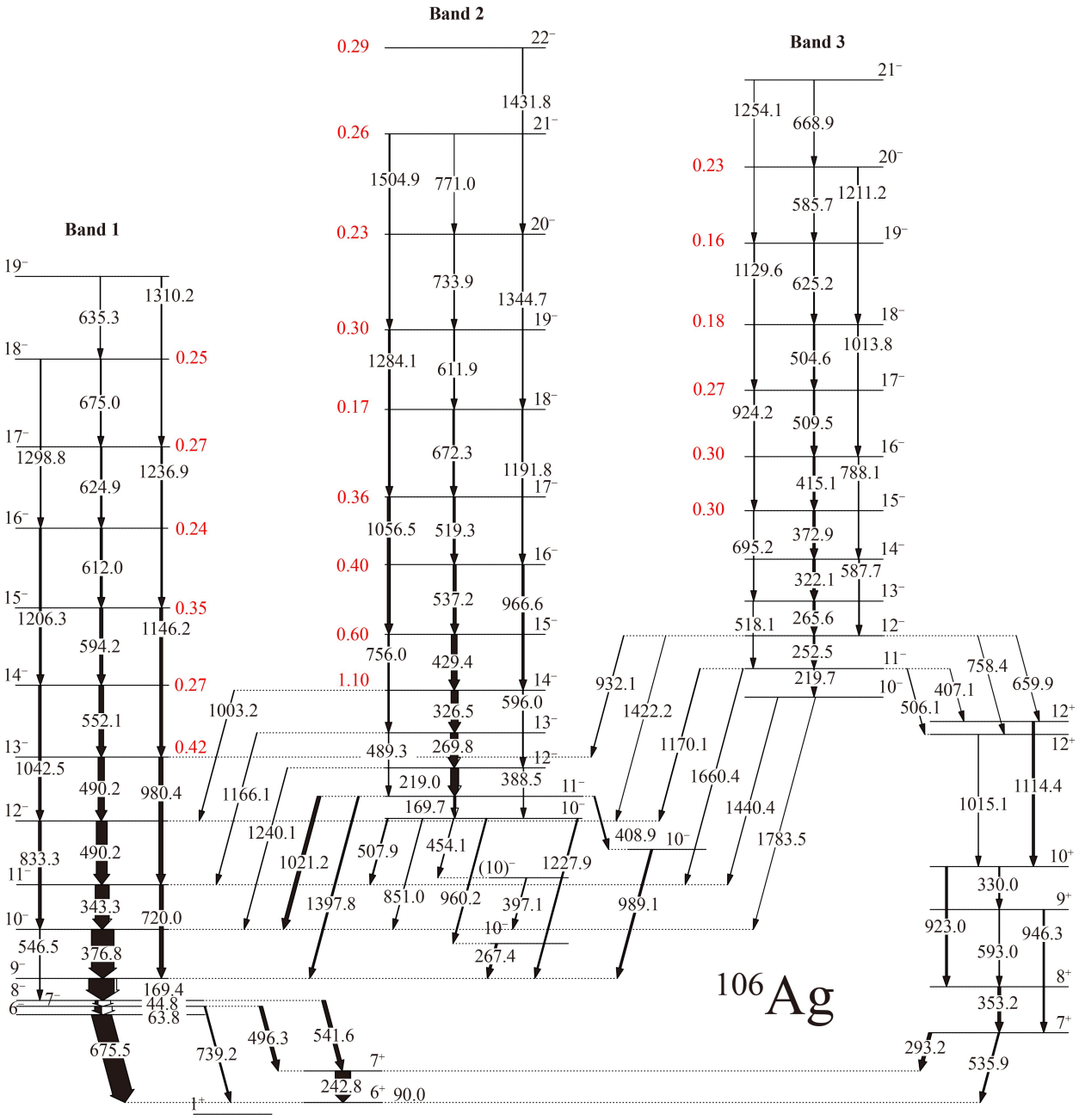

Fig. 30 Partial level scheme of ^{106}Ag [24]. The widths of the arrows represent the relative intensities of the transitions. The lifetimes, in ps, are indicated in red; their uncertainties are, on average, 20%.

bands had been ruled out. It should be noted that this conclusion also differed from a contemporary work by Rather *et al.* [81].

7 Pseudo spin and reflection asymmetry

7.1 Chiral bands and octupole correlations

The atomic nucleus, as a many-body quantum system, carries a wealth of information on fundamental symmetries and symmetry breaking. Besides chiral symmetry, reflection symmetry also plays a very important role in atomic nuclei. Octupole correlations are a manifestation of broken reflection symmetry in the nuclear mean field [82], an effect that develops when the valence nucleons occupy states of opposite parity with both orbital and total angular momenta differing by $3\hbar$. The conditions are satisfied for proton (neutron) number $Z(N) = 34$, 56, 88 and 134 [82]. It is very interesting to explore new phenomena that arise when chiral and reflection symmetries coexist in a single nucleus.

In 2016, Liu *et al.* [20] were the first to report the new

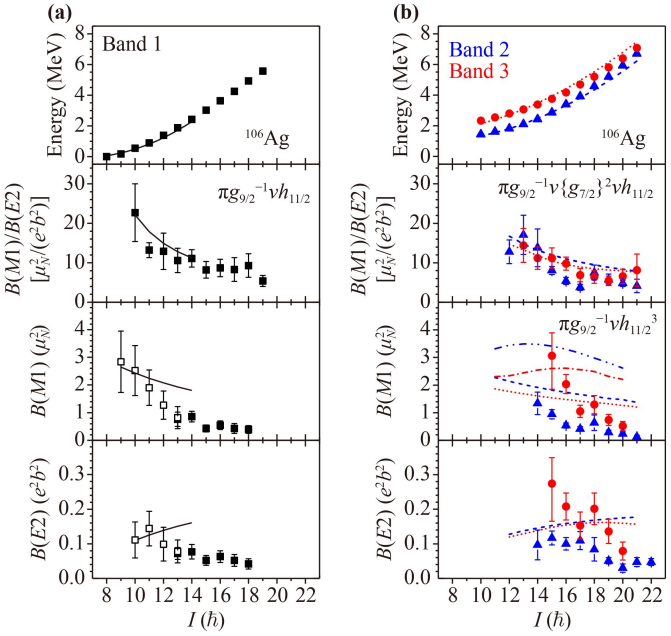

Fig. 31 Comparison of experimental (symbols) and calculated (lines) excitation energies and electromagnetic transition properties of **(a)** Band 1 and **(b)** Bands 2 and 3 [24]. The open squares for Band 1 indicate results from Ref. [80]. The theoretical results for $\pi g_{9/2}^{-1}\otimes\nu g_{7/2}^2\nu h_{11/2}$ configurations of Bands 2 and 3 are displayed as dashed and dotted lines, respectively. The $BM1$ values of bands 2 and 3 are also compared with calculations using a configuration, shown as dash–dot–dotted and dash–dotted lines, respectively.

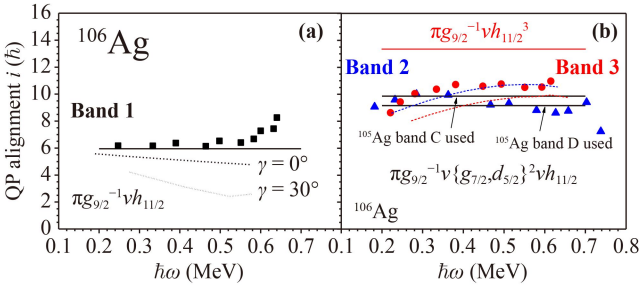

Fig. 32 Quasiparticle alignment i as function of rotational frequency for **(a)** Band 1 and **(b)** Bands 2 and 3 in ^{106}Ag. The experimental points are shown as full symbols. The alignments deduced from the neighbouring nuclei are indicated as straight lines. Results of theoretical calculations are displayed as dashed and dotted lines. The Harris parameters are $\Im_0 = 8.9\hbar^2$ MeV^{-1} and $\Im_1 = 15.7\hbar^4$ MeV^{-3}. Reproduced from Ref. [24].

phenomenon of the coexistence of chirality and octupole correlations. Medium- and high-spin states in ^{78}Br were investigated using in-beam γ spectroscopy using the AFRODITE array (Table 1). Figure 33 shows the level scheme of ^{78}Br and the experimental data in comparison with TPRM calculations. Two pairs of positive- and negative-parity doublet bands together with eight strong electric dipole transitions linking their yrast positive- and negative-parity bands were identified. The positive-parity doublet bands (Bands 1 and 2) and the negative-parity doublet bands (Bands 3 and 4) were proposed to have configurations $\pi g_{9/2}\otimes\nu g_{9/2}$ and $\pi f_{5/2}\otimes\nu g_{9/2}$, respectively. As shown in Fig. 33, the small energy differences between Bands 1, 2 and Bands 3, 4 are well reproduced by the TPRM calculations, as are the magnitude and trend of the energy staggering parameters $S(I)$ and $B(M1)/B(E2)$ ratios. Thus, the configuration assignments and the interpretation of Multiple Chiral Doublet (MχD) bands are supported by the good agreement between the theoretical calculations and the experimental data. It should be noted that the deviation from the data for the $S(I)$ values and $B(M1)/B(E2)$ ratios of Band 3 might be attributed to the neglect of mixing between the $f_{5/2}$ and $p_{3/2}$ orbitals in the TPRM calculations.

The observation of eight $E1$ transitions between positive-parity Band 1 and negative-parity Band 3 (see Fig. 33), implies the existence of octupole correlations. As the proton number of ^{78}Br is close to 34, where the octupole interaction between the $\pi g_{9/2}$ and the $\pi p_{3/2}$ orbitals gives rise to octupole correlations, it was suggested [20] that for the $\pi f_{5/2}\otimes\nu g_{9/2}$ band, the $\pi f_{5/2}$ orbital is actually mixed with the $\pi p_{3/2}$ orbital, leading to octupole interactions and E1 transitions between the chiral bands. The experimental $B(E1)/B(E2)$ branching ratios and the energy displacement δE between Bands 1 and 3 in ^{78}Br are compared with those of ^{224}Th [83] and ^{125}Ba [84] in Fig. 34. The alternating parity band in ^{224}Th is understood as an example of stable octupole deformation [83], while the positive- and negative-parity bands connected by E1 transitions in ^{125}Ba have been interpreted as evidence of octupole correlations [84]. As shown in Fig. 34, the $B(E1)/B(E2)$ branching ratios and δE in ^{78}Br are comparable with those in ^{125}Ba, but deviate appreciably from those in ^{224}Th. So while stable octupole shape can be discounted in ^{78}Br, the features nonetheless indicate the existence of octupole correlations. In Fig. 34, the $B(E1)/B(E2)$ branching ratios increase with spin in ^{78}Br. The δE stays constant for even spin, whereas for odd spin it decreases dramatically, leading to an average decreasing trend. Both features indicate that the octupole correlations enhance with spin in ^{78}Br.

Thus Liu *et al.* [20] observed MχD bands with octupole correlations in ^{78}Br, which provided the first example of chiral geometry in octupole soft nuclei and indicated that chirality and octupole correlations can coexist in a single nucleus. It motivates further experimental studies of the coexistence of multiple symmetries in a single nucleus and encourages the theoretical exploration of the reflection-asymmetric triaxial nucleus.

Recently, a new example of the coexistence of chirality and octupole correlations in the nucleus, ^{74}As was reported by Xiao *et al.* [19]. High-spin states of ^{74}As were populated via the reaction ^{74}Ge(^{4}He, $1p3n$) as

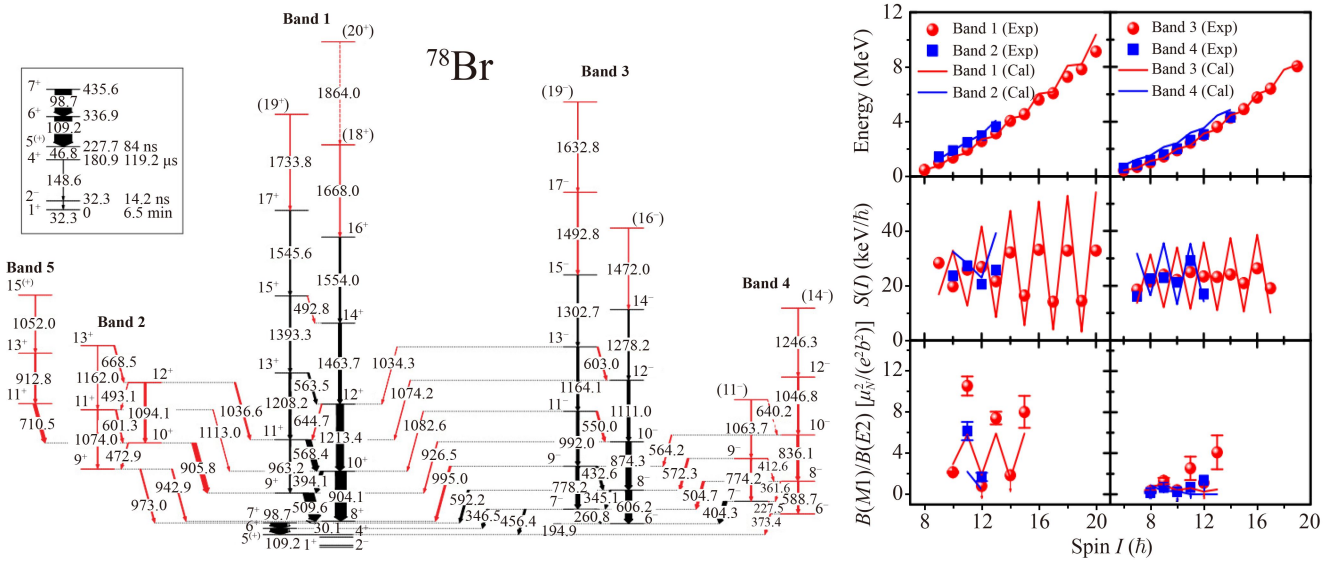

Fig. 33 The level scheme of ^{78}Br (left panel) and the experimental excitation energies, energy staggering parameters $S(I) = [E(I) - E(I-1)]/2I$, and reduced transition probability ratios $B(M1)/B(E2)$ for MχD in ^{78}Br in comparison with the TPRM calculations (right panel). Reproduced from Ref. [20].

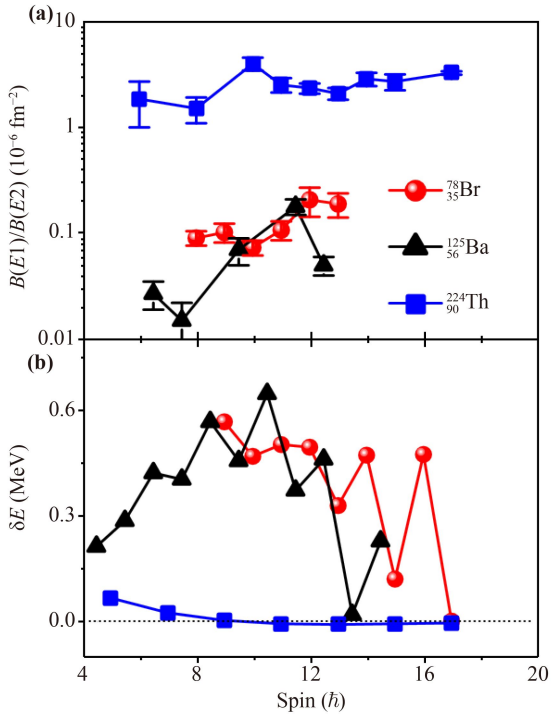

Fig. 34 The experimental $B(E1)/B(E2)$ values **(a)** and energy displacement δE **(b)** between Bands 1 and 3 as functions of spin in ^{78}Br, together with those in ^{125}Ba [84] and ^{224}Th [83].

detailed in Table 1. Figure 35 shows the level scheme of ^{74}As and the available experimental data in comparison with TPRM calculations. One negative-parity and two positive-parity bands were identified. Among them, the two positive-parity bands (1 and 2) were suggested to have the configuration $\pi g_{9/2} \otimes \nu g_{9/2}$ – the same as the chiral configuration in ^{78}Br. As shown in Fig. 35, Bands 1 and 2 maintain an energy difference of ≈ 400 keV over the observed spin range. The two bands have similar $S(I)$ values and exhibit a smooth variation of $S(I)$ as a function of spin. The $B(M1)/B(E2)$ values of the doublet bands are similar and show odd–even staggering. As these features are consistent with the fingerprints of the chiral doublet bands, Bands 1 and 2 were suggested as a pair of chiral doublet bands with the $\pi g_{9/2} \otimes \nu g_{9/2}$ configuration. In addition, the above experimental features are in good agreement with the TPRM calculations as shown in Fig. 35. This agreement supports the configuration assignment and interpretation of the doublet bands.

The work placed three new E1 transitions linking positive-parity Band 1 to negative-parity Band 3, implying the existence of octupole correlations in ^{74}As. The experimental $B(E1)/B(E2)$ values and energy displacement δE between Bands 1 and 3 are shown in Fig. 36. It can be seen that the $B(E1)/B(E2)$ and δE values in ^{74}As are comparable with those in ^{78}Br. These features suggest that octupole correlations also exist in ^{74}As. The proton number ($Z = 33$) in ^{74}As is closer to 34 than the neutron number ($N = 41$), so the occurrence of octupole correlations in ^{74}As are more likely to result from valence protons occupying the $\pi g_{9/2}$ and $\pi p_{3/2}$ orbitals.

7.2 Chiral bands and pseudo spin

The 2016 observation [20] of MχD with octupole correlations in odd–odd ^{78}Br indicated that a simultaneous breaking of chirality and reflection symmetries may exist

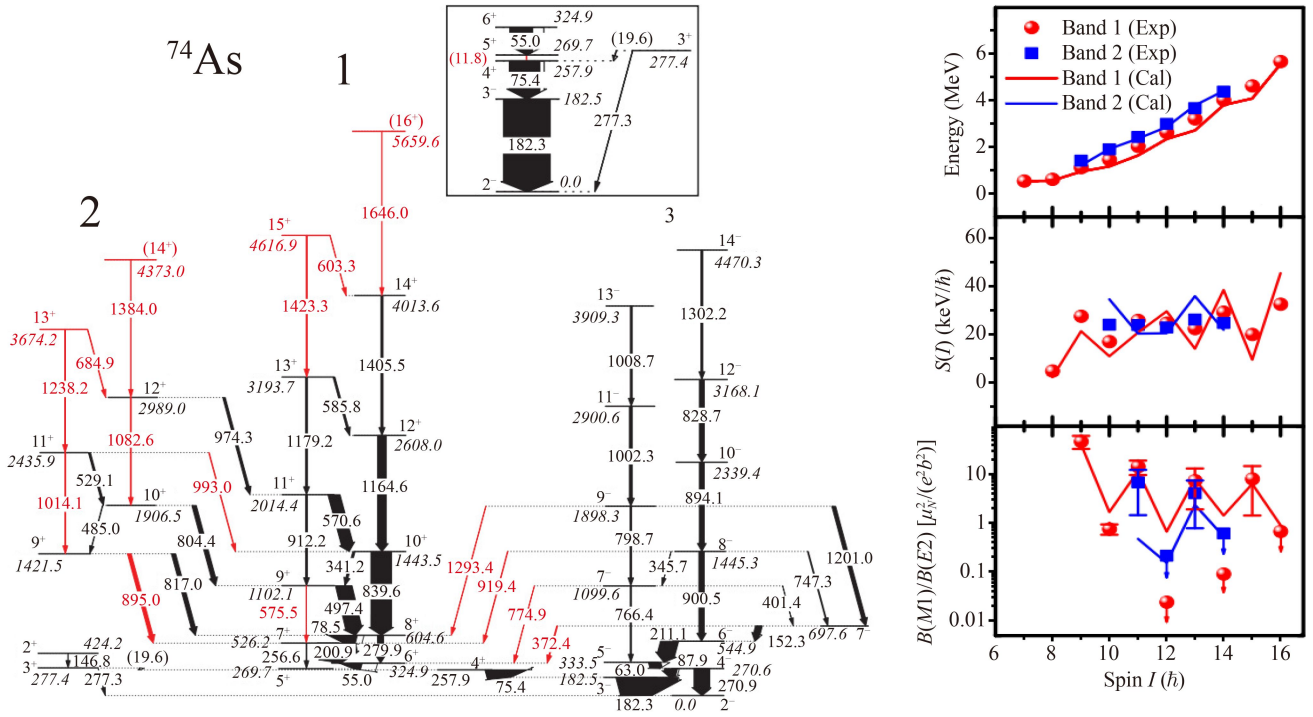

Fig. 35 The level scheme of ^{74}As (left panel) and the experimental excitation energies, energy staggering parameters $S(I) = [E(I) - E(I-1)]/2I$, and reduced transition probability ratios $B(M1)/B(E2)$ for chiral doublet bands in ^{74}As in comparison with the TPRM calculations (right panel). Reproduced from Ref. [19].

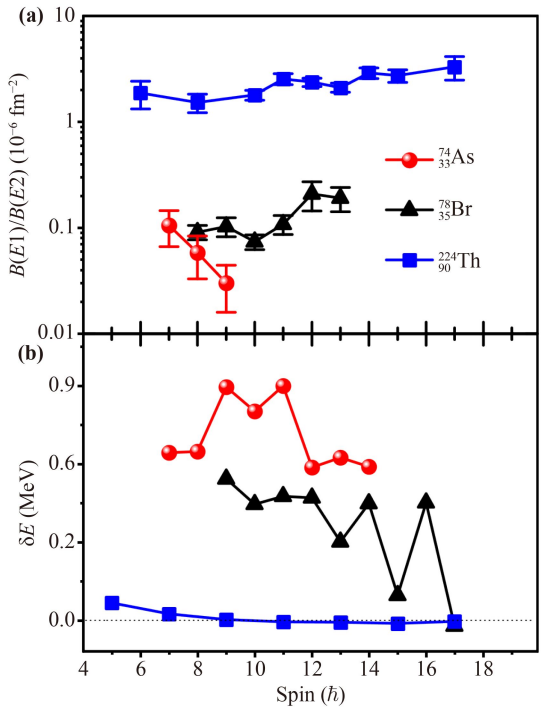

Fig. 36 The experimental $B(E1)/B(E2)$ values **(a)** and energy displacement δE **(b)** between Bands 1 and 3 in ^{74}As, as functions of spin, together with those in ^{78}Br and ^{224}Th [83].

in nuclei. The work motivated further studies of the coexistence of multiple symmetries in a single nucleus [85]. Recently, the coexistence of broken chiral symmetry and pseudospin symmetry has attracted significant attention. Pseudospin symmetry in atomic nuclei was introduced [86, 87] to explain the near degeneracy of two states with quantum numbers $(n, l, j = l + 1/2)$ and $(n-1, l+2, j = l + 3/2)$ – the pseudospin doublets.

In 2019, Jia *et al.* [88] presented calculations for the three nearly degenerate bands with the $\pi g_{9/2}^{-1} \otimes \nu h_{11/2}(d_{5/2}, g_{7/2})$ configuration in ^{105}Ag, performed using the CDFT and the Multiparticle Plus Rotor Model (MPRM). The results suggested that these three bands were pseudospin-chiral triplet bands. It pointed to the possibility of pseudospin-chiral quartet bands existing in atomic nuclei. Subsequently, such quartet bands with the $\pi h_{11/2}(d_{5/2}, g_{7/2}) \otimes \nu h_{11/2}$ configuration were found in ^{131}Ba [89]. The pseudospin-chiral triplet and quartet bands mentioned above both involve the $(d_{5/2}, g_{7/2})$ pseudospin doublet. Thus, it is of scientific interest to explore pseudospin-chiral triplet (or quartet) bands based on other pseudospin doublets.

Recently, Mu *et al.* [22] reported the first example of pseudospin-chiral triplet bands involving the $\pi(p_{3/2}, f_{5/2})$ pseudospin doublet. In this work, medium- and high-spin states in the odd-A nucleus ^{81}Kr were studied via fusion evaporation reactions at iThemba LABS (see Table 1). Figure 37 shows the level scheme of ^{81}Kr. Two nearly degenerate positive-parity bands (2 and 3) with the $\pi g_{9/2}^2 \otimes \nu g_{9/2}^{-1}$ configuration and three nearly degenerate negative-parity Bands (5, 6 and 7) with the

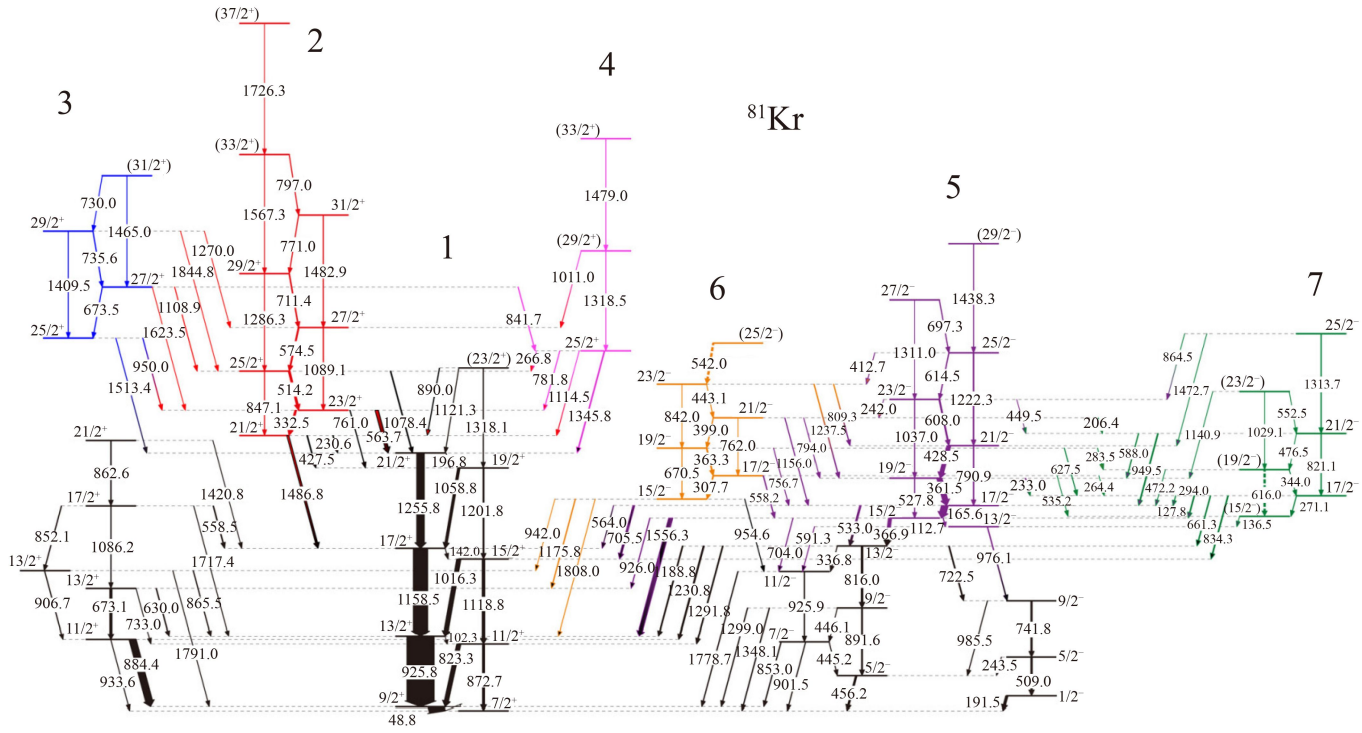

Fig. 37 Level scheme of ^{81}Kr [22].

$\pi g_{9/2}(p_{3/2}, f_{5/2}) \otimes \nu g_{9/2}^{-1}$ configuration were identified. Figure 38 presents the excitation energies $E(I)$ and the $B(M1)/B(E2)$ ratios for these bands. As shown in Figs. 38(a1) and (a2), for Bands 2 and 3, the $E(I)$ values are close to each other; the $B(M1)/B(E2)$ ratios are similar and show odd–even staggering with the same phase as a function of spin. These behaviours are consistent with the fingerprints of chiral doublet bands. Similarly, Bands 5 and 6 also exhibited the expected properties of chiral doublet bands as shown in Figs. 38(b1) and (b2). Therefore, Bands 2 & 3 and Bands 5 & 6 are likely to be two pairs of chiral doublet bands. However, in Fig. 38(c2),

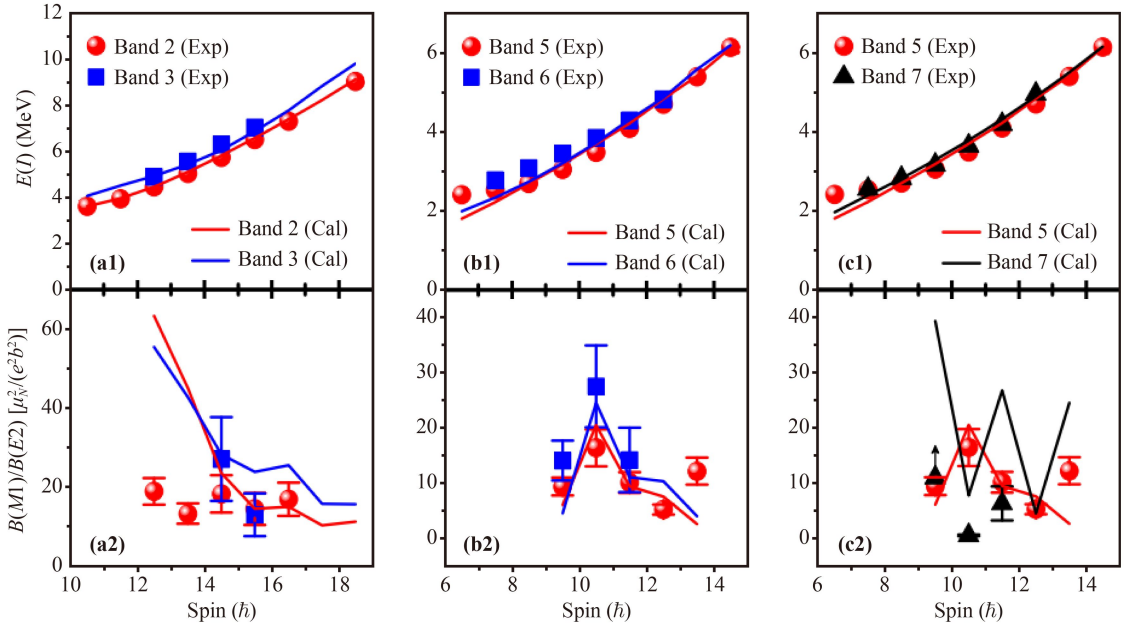

Fig. 38 The experimental $E(I)$ and $B(M1)/B(E2)$ for bands 2, 3 with the $\pi g_{9/2}^2 \otimes \nu g_{9/2}^{-1}$ configuration and bands 5, 6, 7 with the $\pi g_{9/2}(p_{3/2}, f_{5/2}) \otimes \nu g_{9/2}^{-1}$ configuration in ^{81}Kr in comparison with the MPRM results [22].

Bands 5 and 7 exhibit the opposite phase in the $B(M1)/B(E2)$ staggering, which is consistent with the characteristic of pseudospin doublet bands proposed in Refs. [90, 91]. Thus, Bands 6 and 7 were suggested as the chiral partner and the pseudospin partner of Band 5, respectively. From the signature argument, the largest component of the configuration for Bands 5 and 6 would be $\pi g_{9/2}p_{3/2} \otimes \nu g_{9/2}^{-1}$, whereas for Band 7 it would be $\pi g_{9/2}f_{5/2} \otimes \nu g_{9/2}^{-1}$.

The MPRM calculations for Bands 2, 3, 5, 6 and 7, in comparison with the available data, are also shown in Fig. 38. The characteristics of the experimental data were reproduced by the MPRM calculations. The agreement between the calculated values and the corresponding experimental data provides additional support for the configuration assignments and interpretations of these bands. Thus, based on the experimental features and theoretical calculations, Bands 2 and 3 as well as Bands 5 and 6 are interpreted as chiral doublet bands, and Band 7 is interpreted as the pseudospin partner of Band 5. These observations presented the two new chiral configurations – $\pi g_{9/2}^2 \otimes \nu g_{9/2}^{-1}$ and $\pi g_{9/2}(p_{3/2}, f_{5/2}) \otimes \nu g_{9/2}^{-1}$ – and the first example of pseudospin-chiral triplet bands involving the $(p_{3/2}, f_{5/2})$ pseudospin doublet.

8 Summary

The AFRODITE array has been used by local and Chinese groups to discover new regions of chirality around mass 80 and 190. Many phenomena have been observed, such as multiple chiral bands, three and four quasiparticle chiral bands, very close degeneracies, octupole correlations and chiral bands, and pseudo-spin chiral structures.

To understand the chiral bands, particle-rotor model calculations were made to compare measured quantities such as energies, $B(M1)/B(E2)$ ratios, absolute transition rates, and energy staggering to the model. The model calculations also allowed one to draw conclusions about the orientation of the angular-momentum vectors of the proton, neutron and core components to judge whether observed bands conformed to static chirality, or chiral vibration. Studies of the features of chiral bands calculated with the quasiparticle-plus-triaxial-rotor model indicated that the fingerprints for broken chiral symmetry in the intrinsic frame are too restrictive and may miss the identification of some bands as chiral. The expectations for (i) degeneracy in the energies, alignments, moments of inertia, and $B(M1)$, $B(E2)$ transitions probabilities, (ii) lack of energy staggering, and (iii) specific staggering in the $B(M1)$ transition probabilities, appear in the calculations only in simplified model description, where the single-particle angular momenta are fixed along the short and long nuclear axes. It was also shown that chiral geometry may form for many-particle nuclear systems where the single-particle angular momenta along the short and long nuclear axes differ substantially.

According to the particle-rotor model, the nuclei ^{80}Br and ^{82}Br exhibit chiral vibration and static chirality, respectively. In ^{78}Br MχD bands were observed having opposite parity. Transitions linking these bands indicated the presence of octupole correlations. The level scheme of ^{106}Ag has been revisited and interpreted in terms of two- and four-quasiparticle bands. In ^{81}Kr MχD bands were observed but in this instance they were associated with pseudo-spin partners. The nucleus ^{198}Tl was the first case of nuclear chirality reported in the mass 190 region, while ^{193,194}Tl, exhibited multiple bands based on two, three or four quasiparticle configurations. The four quasiparticle chiral pair in ^{194}Tl showed the best example of chiral degeneracy.

Declarations The authors declare that they have no competing interests and there are no conflicts.

Acknowledgements The authors gratefully thank the numerous members of the iThemba LABS technical staff and accelerator group for their support. This work was supported by the National Research Foundation of South Africa under Grant Nos. 65268, 65581, 75248, 75357, 76632, 80977, 88646, 90741, 91446, 92791, 92792, 93531, 103478, 109134 and 116666, the Outstanding Youth Fund of the Natural Science Foundation of Shandong Province (No. ZR2020YQ07), and the National Natural Science Foundation of China (Nos. U2167202, 12075137, 12075138, and 12225504).

References and notes

1. S. Frauendorf and J. Meng, Tilted rotation of triaxial nuclei, *Nucl. Phys. A* 617(2), 131 (1997)
2. B. W. Xiong and Y. Y. Wang, Nuclear chiral doublet bands data tables, *At. Data Nucl. Data Tables* 125, 193 (2019)
3. E. A. Lawrie and O. Shirinda, Reaching degeneracy in two-quasiparticle chiral bands, *Phys. Lett. B* 689(2-3), 66 (2010)
4. P. B. Semmes and I. Ragnarsson, in: J. X. Saladin, R. A. Sorenson, and C. M. Vincent (Eds.), Proc. Int. Conf. on High-Spin Physics and Gamma-Soft Nuclei, Pittsburgh, 1990, World Scientific, 1991, p. 500
5. P. B. Semmes and I. Ragnarsson, in: J. Dudek and B. Haas (Eds.), Proc. Future Directions in Nuclear Physics with 4π Gamma Detection Systems of the New Generation, in: *AIP Conf. Proc.* 259(566), 1992
6. O. Shirinda and E. A. Lawrie, Identifying chiral bands in real nuclei, *Eur. Phys. J. A* 48(9), 118 (2012)
7. T. Koike, K. Starosta, and I. Hamamoto, Chiral bands, dynamical spontaneous symmetry breaking, and the selection rule for electromagnetic transitions in the chiral geometry, *Phys. Rev. Lett.* 93(17), 172502 (2004)
8. C. Vaman, D. B. Fossan, T. Koike, K. Starosta, I. Y. Lee, and A. O. Macchiavelli, Chiral degeneracy in triaxial

^{104}Rh, *Phys. Rev. Lett.* 92(3), 032501 (2004)
9. S. Mukhopadhyay, D. Almehed, U. Garg, S. Frauendorf, T. Li, P. V. M. Rao, X. Wang, S. S. Ghugre, M. P. Carpenter, S. Gros, A. Hecht, R. V. F. Janssens, F. G. Kondev, T. Lauritsen, D. Seweryniak, and S. Zhu, From chiral vibration to static chirality in ^{135}Nd, *Phys. Rev. Lett.* 99(17), 172501 (2007)
10. P. L. Masiteng, E. A. Lawrie, T. M. Ramashidzha, R. A. Bark, B. G. Carlsson, J. J. Lawrie, R. Lindsay, F. Komati, J. Kau, P. Maine, S. M. Maliage, I. Matamba, S. M. Mullins, S. H. T. Murray, K. P. Mutshena, A. A. Pasternak, I. Ragnarsson, D. G. Roux, J. F. Sharpey-Schafer, O. Shirinda, and P. A. Vymers, Close near-degeneracy in a pair of four-quasiparticle bands in 194Tl, *Phys. Lett. B* 719(1–3), 83 (2013)
11. O. Shirinda, E. A. Lawrie, and B. G. Carlsson, Can a chiral system be built on a strongly asymmetric nucleon configuration? *Acta Phys. Pol. B* 44(3), 341 (2013)
12. B. G. Carlsson and I. Ragnarsson, Many-particles–plus–rotor description of magnetic bands at high spin, *Phys. Rev. C Nucl. Phys.* 74(4), 044310 (2006)
13. O. Shirinda and E. A. Lawrie, Multiple many-particle chiral systems described within the particle-rotor model, *Eur. Phys. J. A* 52(11), 344 (2016)
14. O. Shirinda and E. A. Lawrie, Multiple chiral bands built on the same many-particle nucleon configuration in the 100 mass region, *Acta Phys. Pol. B Proc. Suppl.* 11(1), 149 (2018)
15. E. A. Lawrie, Decay patterns of multi-quasiparticle bands — a model independent test of chiral symmetry, *Phys. Scr.* 92(9), 094006 (2017)
16. R. Bass, Nuclear Reactions with Heavy Ions, Springer Verlag, Berlin, Heidelberg, New York, 1980
17. R. Schwengner, F. Dönau, T. Servene, H. Schnare, J. Reif, G. Winter, L. Käubler, H. Prade, S. Skoda, J. Eberth, H. G. Thomas, F. Becker, B. Fiedler, S. Freund, S. Kasemann, T. Steinhardt, O. Thelen, T. Härtlein, C. Ender, F. Köck, P. Reiter, and D. Schwalm, Magnetic and collective rotation in ^{79}Br, *Phys. Rev. C* 65(4), 044326 (2002)
18. J. S. Dionisio, R. Meunier, C. Schück, C. Vieu, J. M. Lagrange, M. Pautrat, J. C. S. Bacelar, J. R. Jongman, W. R. Phillips, J. L. Durell, W. Urban, B. J. Varley, and H. Folger, Target structure and in-beam electron spectra, *Nucl. Instrum. Methods Phys. Res. A* 362(1), 122 (1995)
19. X. Xiao, S. Y. Wang, C. Liu, R. A. Bark, J. Meng, S. Q. Zhang, B. Qi, H. Hua, P. Jones, S. M. Wyngaardt, S. Wang, D. P. Sun, Z. Q. Li, N. B. Zhang, H. Jia, R. J. Guo, X. C. Han, L. Mu, X. Lu, W. Z. Xu, C. Y. Niu, C. G. Wang, E. A. Lawrie, J. J. Lawrie, J. F. Sharpey-Schafer, M. Wiedeking, S. N. T. Majola, T. D. Bucher, T. Dinoko, B. Maqabuka, L. Makhathini, L. Mdletshe, N. A. Khumalo, O. Shirinda, and K. Sowazi, Chirality and octupole correlations in ^{74}As, *Phys. Rev. C* 106(6), 064302 (2022)
20. C. Liu, S. Y. Wang, R. A. Bark, S. Q. Zhang, J. Meng, B. Qi, P. Jones, S. M. Wyngaardt, J. Zhao, C. Xu, S. G. Zhou, S. Wang, D. P. Sun, L. Liu, Z. Q. Li, N. B. Zhang, H. Jia, X. Q. Li, H. Hua, Q. B. Chen, Z. G. Xiao, H. J. Li, L. H. Zhu, T. D. Bucher, T. Dinoko, J. Easton, K. Juhász, A. Kamblawe, E. Khaleel, N. Khumalo, E. A. Lawrie, J. J. Lawrie, S. N. T. Majola, S. M. Mullins, S. Murray, J. Ndayishimye, D. Negi, S. P. Noncolela, S. S. Ntshangase, B. M. Nyakó, J. N. Orce, P. Papka, J. F. Sharpey-Schafer, O. Shirinda, P. Sithole, M. A. Stankiewicz, and M. Wiedeking, Evidence for octupole correlations in multiple chiral doublet bands, *Phys. Rev. Lett.* 116(11), 112501 (2016)
21. S. Y. Wang, B. Qi, L. Liu, S. Q. Zhang, H. Hua, X. Q. Li, Y. Y. Chen, L. H. Zhu, J. Meng, S. M. Wyngaardt, P. Papka, T. T. Ibrahim, R. A. Bark, P. Datta, E. A. Lawrie, J. J. Lawrie, S. N. T. Majola, P. L. Masiteng, S. M. Mullins, J. Gál, G. Kalinka, J. Molnár, B. M. Nyakó, J. Timár, K. Juhász, and R. Schwengner, The first candidate for chiral nuclei in the $A \sim 80$ mass region: ^{80}Br, *Phys. Lett. B* 703(1), 40 (2011)
22. L. Mu, S. Y. Wang, C. Liu, B. Qi, R. A. Bark, J. Meng, S. Q. Zhang, P. Jones, S. M. Wyngaardt, H. Jia, Q. B. Chen, Z. Q. Li, S. Wang, D. P. Sun, R. J. Guo, X. C. Han, W. Z. Xu, X. Xiao, P. Y. Zhu, H. W. Li, H. Hua, X. Q. Li, C. G. Li, R. Han, B. H. Sun, L. H. Zhu, T. D. Bucher, B. V. Kheswa, N. Khumalo, E. A. Lawrie, J. J. Lawrie, K. L. Malatji, L. Msebi, J. Ndayishimye, J. F. Sharpey-Schafer, O. Shirinda, M. Wiedeking, T. Dinoko, and S. S. Ntshangase, First observation of the coexistence of multiple chiral doublet bands and pseudospin doublet bands in the $A \approx 80$ mass region, *Phys. Lett. B* 827, 137006 (2022)
23. C. Liu, S. Y. Wang, B. Qi, S. Wang, D. P. Sun, Z. Q. Li, R. A. Bark, P. Jones, J. J. Lawrie, L. Masebi, M. Wiedeking, J. Meng, S. Q. Zhang, H. Hua, X. Q. Li, C. G. Li, R. Han, S. M. Wyngaardt, B. H. Sun, L. H. Zhu, T. D. Bucher, B. V. Kheswa, K. L. Malatji, J. Ndayishimye, O. Shirinda, T. Dinoko, N. Khumalo, E. A. Lawrie, and S. S. Ntshangase, New candidate chiral nucleus in the $A \approx 80$ mass region: ^{47,35,82}Br, *Phys. Rev. C* 100(5), 054309 (2019)
24. E. O. Lieder, R. M. Lieder, R. A. Bark, Q. B. Chen, S. Q. Zhang, J. Meng, E. A. Lawrie, J. J. Lawrie, S. P. Bvumbi, N. Y. Kheswa, S. S. Ntshangase, T. E. Madiba, P. L. Masiteng, S. M. Mullins, S. Murray, P. Papka, D. G. Roux, O. Shirinda, Z. H. Zhang, P. W. Zhao, Z. P. Li, J. Peng, B. Qi, S. Y. Wang, Z. G. Xiao, and C. Xu, Resolution of chiral conundrum in ^{106}Ag: Doppler-shift lifetime investigation, *Phys. Rev. Lett.* 112(20), 202502 (2014)
25. J. Ndayishimye, E. A. Lawrie, O. Shirinda, J. L. Easton, J. J. Lawrie, S. M. Wyngaardt, R. A. Bark, T. D. Bucher, S. P. Bvumbi, T. R. S. Dinoko, P. Jones, N. Y. Kheswa, S. N. T. Majola, P. L. Masiteng, D. Negi, J. N. Orce, J. F. Sharpey-Schafer, and M. Wiedeking, Competition of rotation around the intermediate and long axes in ^{193}Tl, *Phys. Rev. C* 100(1), 014313 (2019)
26. P. L. Masiteng, E. A. Lawrie, T. M. Ramashidzha, J. J. Lawrie, R. A. Bark, R. Lindsay, F. Komati, J. Kau, P. Maine, S. M. Maliage, I. Matamba, S. M. Mullins, S. H. T. Murray, K. P. Mutshena, A. A. Pasternak, D. G. Roux, J. F. Sharpey-Schafer, O. Shirinda, and P. A. Vymers, Rotational bands and chirality in ^{194}Tl, *Eur. Phys. J. A* 50(7), 119 (2014)
27. P. L. Masiteng, A. A. Pasternak, E. A. Lawrie, O. Shirinda, J. J. Lawrie, R. A. Bark, S. P. Bvumbi, N. Y.

Kheswa, R. Lindsay, E. O. Lieder, R. M. Lieder, T. E. Madiba, S. M. Mullins, S. H. T. Murray, J. Ndayishimye, S. S. Ntshangase, P. Papka, and J. F. Sharpey-Schafer, Sharpey-Schafer, DSAM lifetime measurements for the chiral pair in ^{194}Tl, *Eur. Phys. J. A* 52(2), 28 (2016)

28. E. A. Lawrie, P. A. Vymers, J. J. Lawrie, Ch. Vieu, R. A. Bark, R. Lindsay, G. K. Mabala, S. M. Maliage, P. L. Masiteng, S. M. Mullins, S. H. T. Murray, I. Ragnarsson, T. M. Ramashidza, C. Shück, J. F. Sharpey-Schafer, and O. Shirinda, Possible chirality in the doubly-odd ^{198}Tl nucleus: Residual interaction at play, *Phys. Rev. C* 78, 021305(R) (2008)
29. E. A. Lawrie, P. A. Vymers, Ch. Vieu, J. J. Lawrie, C. Schück, R. A. Bark, R. Lindsay, G. K. Mabala, S. M. Maliage, P. L. Masiteng, S. M. Mullins, S. H. T. Murray, I. Ragnarsson, T. M. Ramashidzha, J. F. Sharpey-Schafer, and O. Shirinda, Candidate chiral bands in ^{198}Tl, *Eur. Phys. J. A* 45(1), 39 (2010)
30. J. L. Conradie, et al., New Developments at iThemba LABS, in: Proc. CYC'16, Zurich, Switzerland, 2016, pp 274–277
31. P. Sortais, Recent progress in making highly charged ion beams, *Nucl. Instrum. Methods Phys. Res. B* 98(1–4), 508 (1995)
32. H. Waldmann and B. Martin, Highly charged metal ion beams produced from organometallic compounds, *Nucl. Instrum. Methods Phys. Res. B* 98(1–4), 532 (1995)
33. D. Hitz, D. Cormier, and J. M. Mathonnet, Proc. EPAC'02, Paris, France, 2002, paper THPRI005, page 1718
34. R. T. Newman, et al., Proceedings of the Balkan School on Nuclear Physics, *Balkan Phys. Lett.* Special Issue 182, (1998)
35. J. F. Sharpey-Schafer, Laboratory portrait: iThemba laboratory for accelerator-based sciences, *Nucl. Phys. News* 14(1), 5 (2004)
36. M. Moszyński and G. Duchêne, Ballistic deficit correction methods for large Ge detectors, *Nucl. Instrum. Methods Phys. Res. A* 308(3), 557 (1991)
37. P. J. Nolan, G. A. Beck, and D. B. Fossan, Large arrays of escape-suppressed gamma-ray detectors, *Annu. Rev. Nucl. Part. Sci.* 44(1), 561 (1994)
38. R. M. Lieder, Experimental Techniques in Nuclear Physics, Ed. D. N. Poenaru and W. Greiner, Walter de Gruyter, Berlin, 1997, page 137
39. URL: xia.com/products/pixie-16/
40. K. S. Krane, R. M. Steffen, and R. M. Wheeler, Directional correlations of gamma radiations emitted from nuclear states oriented by nuclear reactions or cryogenic methods, *At. Data Nucl. Data Tables* 11(5), 351 (1973)
41. L. W. Fagg and S. S. Hanna, Polarization measurements on nuclear gamma rays, *Rev. Mod. Phys.* 31(3), 711 (1959)
42. K. Starosta, T. Morek, C. Droste, S. G. Rohoziński, J. Srebrny, A. Wierzchucka, M. Bergström, B. Herskind, E. Melby, T. Czosnyka, and P. J. Napiorkowski, Experimental test of the polarization direction correlation method (PDCO), *Nucl. Instrum. Methods Phys. Res. A* 423(1), 16 (1999)
43. E. O. Lieder, A. A. Pasternak, R. M. Lieder, A. D. Efimov, V. M. Mikhajlov, B. G. Carlsson, I. Ragnarsson, W. Gast, T. Venkova, T. Morek, S. Chmel, G. de Angelis, D. R. Napoli, A. Gadea, D. Bazzacco, R. Menegazzo, S. Lunardi, W. Urban, C. Droste, T. Rzaca-Urban, G. Duchêne, and A. Dewald, Investigation of lifetimes in quadrupole bands of ^{142}Gd, *Eur. Phys. J. A* 35(2), 135 (2008)
44. R. M. Lieder, A. A. Pasternak, E. O. Podsvirova, A. D. Efimov, V. M. Mikhajlov, R. Wyss, T. Venkova, W. Gast, H. M. Jäger, L. Mihailescu, D. Bazzacco, S. Lunardi, R. Menegazzo, C. Rossi Alvarez, G. de Angelis, D. R. Napoli, T. Rzaca-Urban, W. Urban, and A. Dewald, Investigations of the level scheme of ^{144}Gd and lifetimes in the quadrupole bands, *Eur. Phys. J. A* 21(1), 37 (2004)
45. E. Grodner, A. A. Pasternak, C. Droste, T. Morek, J. Srebrny, J. Kownacki, W. Płóciennik, A. A. Wasilewski, M. Kowalczyk, M. Kisieliński, R. Kaczarowski, E. Ruchowska, A. Kordyasz, and M. Wolińska, Lifetimes and side-feeding population of the yrast band levels in ^{131}La, *Eur. Phys. J. A* 27(3), 325 (2006)
46. T. Belgya, O. Bersillon, R. Capote Noy, T. Fukahori, G. Zhigang, S. Goriely, M. Herman, A. V. Ignatyuk, S. Kailas, A. J. Koning, P. Oblozinsky, V. Plujko, and P. G. Young, Handbook for Calculations of Nuclear Reaction Data, RIPL-2, IAEA-TECDOC-1506, IAEA, Vienna, 2006
47. R. M. Lieder, A. A. Pasternak, E. O. Lieder, W. Gast, G. de Angelis, and D. Bazzacco, Investigation of γ-ray fold distributions in $N \leq 82$ Gd, Eu and Sm nuclei: Observation of a double-humped fold distribution, *Eur. Phys. J. A* 47(9), 115 (2011)
48. J. N. Scheurer, M. Aiche, M. M. Aleonard, G. Barreau, F. Bourgine, D. Boivin, D. Cabaussel, J. F. Chemin, T. P. Doan, J. P. Goudour, M. Harston, A. Brondi, G. La Rana, R. Moro, E. Vardaci, and D. Curien, Improvements in the in-beam γ-ray spectroscopy provided by an ancillary detector coupled to a Ge γ-spectrometer: The DIAMANT-EUROGAM II example, *Nucl. Instrum. Methods Phys. Res. A* 385(3), 501 (1997)
49. J. Gál, G. Hegyesi, J. Molnár, B. M. Nyakó, G. Kalinka, J. N. Scheurer, M. M. Aléonard, J. F. Chemin, J. L. Pedroza, K. Juhász, and V. F. E. Pucknell, The VXI electronics of the DIAMANT particle detector array, *Nucl. Instrum. Methods Phys. Res. A* 516(2–3), 502 (2004)
50. F. S. Komati, R. A. Bark, J. Gál, E. Gueorguieva, K. Juhász, G. Kalinka, A. Krasznahorkay, J. J. Lawrie, M. Lipoglavšek, M. Maliage, J. Molnár, S. M. Mullins, S. H. T. Murray, B. M. Nyakó, M. Ramashidza, J. F. Sharpey-Schafer, J. N. Scheurer, J. Timár, P. Vymers, and L. Zolnai, Commissioning of the DIAMANT "chessboard" light-charged-particle CsI detector array with AFRODITE, *AIP Conf. Proc.* 802, 215 (2005)
51. C. M. Petrache, G. B. Hagemann, I. Hamamoto, and K. Starosta, Risk of misinterpretation of nearly degenerate pair bands as chiral partners in nuclei, *Phys. Rev. Lett.* 96(11), 112502 (2006)
52. D. Tonev, G. de Angelis, P. Petkov, A. Dewald, S. Brant, S. Frauendorf, D. L. Balabanski, P. Pejovic, D. Bazzacco, P. Bednarczyk, F. Camera, A. Fitzler, A. Gadea, S. Lenzi, S. Lunardi, N. Marginean, O. Möller,

D. R. Napoli, A. Paleni, C. M. Petrache, G. Prete, K. O. Zell, Y. H. Zhang, J. Zhang, Q. Zhong, and D. Curien, Transition probabilities in ^{134}Pr: A test for chirality in nuclear systems, *Phys. Rev. Lett.* 96(5), 052501 (2006)

53. K. Starosta, T. Koike, C. J. Chiara, D. B. Fossan, D. R. LaFosse, A. A. Hecht, C. W. Beausang, M. A. Caprio, J. R. Cooper, R. Krücken, J. R. Novak, N. V. Zamfir, K. E. Zyromski, D. J. Hartley, D. L. Balabanski, J. Zhang, S. Frauendorf, and V. I. Dimitrov, Chiral doublet structures in odd–odd $N = 75$ isotones: Chiral vibrations, *Phys. Rev. Lett.* 86(6), 971 (2001)
54. R. A. Bark, A. M. Baxter, A. P. Byrne, G. D. Dracoulis, T. Kibedí, T. R. Mc Goram, and S. M. Mullins, Candidate chiral band in La, *Nucl. Phys. A* 691(3–4), 577 (2001)
55. E. Grodner, J. Srebrny, A. A. Pasternak, I. Zalewska, T. Morek, C. Droste, J. Mierzejewski, M. Kowalczyk, J. Kownacki, M. Kisieliński, S. G. Rohoziński, T. Koike, K. Starosta, A. Kordyasz, P. J. Napiorkowski, M. Wolińska-Cichocka, E. Ruchowska, W. Płóciennik, and J. Perkowski, ^{128}Cs as the best example revealing chiral symmetry breaking, *Phys. Rev. Lett.* 97(17), 172501 (2006)
56. I. Ray, P. Banerjee, S. Bhattacharya, M. Saha-Sarkar, S. Muralithar, R. P. Singh, and R. K. Bhowmik, Structure of positive-parity yrast band in Br, *Nucl. Phys. A* 678(3), 258 (2000)
57. J. Meng, J. Peng, S. Q. Zhang, and S. G. Zhou, Possible existence of multiple chiral doublets in ^{106}Rh, *Phys. Rev. C* 73(3), 037303 (2006)
58. S. Q. Zhang, B. Qi, S. Y. Wang, and J. Meng, Chiral bands for a quasi-proton and quasi-neutron coupled with a triaxial rotor, *Phys. Rev. C* 75(4), 044307 (2007)
59. L. Esser, U. Neuneyer, R. F. Casten, and P. von Brentano, Correlations of the deformation variables β and γ in even–even Hf, W, Os, Pt, and Hg nuclei, *Phys. Rev. C* 55(1), 206 (1997)
60. Y. Tanaka and R. K. Sheline, Comparison of calculated and experimental band structure in odd-A nuclei with $A = 187$–199, *Nucl. Phys. A* 276(1), 101 (1977)
61. J. Meyer-Ter-Vehn, Collective model description of transitional odd-A nuclei, *Nucl. Phys. A* 249(1), 141 (1975)
62. H. Toki, H. L. Yadav, and A. Faessler, Decoupled and strongly coupled particles system in odd–odd mass nuclei, *Phys. Lett. B* 71, 1 (1977)
63. R. A. Bark, J. M. Espino, W. Reviol, P. B. Semmes, H. Carlsson, I. G. Bearden, G. B. Hagemann, H. J. Jensen, I. Ragnarsson, L. L. Riedinger, H. Ryde, and P. O. Tjøm, Signature inversion in semi-decoupled bands: Residual interaction between h_{92} protons and i_{132} neutrons, *Phys. Lett. B* 406(3), 193 (1997) [Erratum: *Phys. Lett. B* 416, 453 (1998)]
64. H. Pai, G. Mukherjee, S. Bhattacharyya, M. R. Gohil, T. Bhattacharjee, C. Bhattacharya, R. Palit, S. Saha, J. Sethi, T. Trivedi, S. Thakur, B. S. Naidu, S. K. Jadav, R. Donthi, A. Goswami, and S. Chanda, High spin band structures in doubly odd ^{194}Tl, *Phys. Rev. C* 85(6), 064313 (2012)
65. R. Bengtsson and S. Frauendorf, Quasiparticle spectra near the yrast line, *Nucl. Phys. A* 327(1), 139 (1979)
66. T. Koike, K. Starosta, C. J. Chiara, D. B. Fossan, and D. R. LaFosse, Systematic search of $\pi h_{11/2} \otimes \nu h_{11/2}$ chiral doublet bands and role of triaxiality in odd–odd $Z = 55$ isotopes: ^{128,130,132,134}Cs, *Phys. Rev. C* 67(4), 044319 (2003)
67. S. Zhu, U. Garg, B. K. Nayak, S. S. Ghugre, N. S. Pattabiraman, D. B. Fossan, T. Koike, K. Starosta, C. Vaman, R. V. F. Janssens, R. S. Chakrawarthy, M. Whitehead, A. O. Macchiavelli, and S. Frauendorf, A composite chiral pair of rotational bands in the odd-A nucleus ^{135}Nd, *Phys. Rev. Lett.* 91(13), 132501 (2003)
68. T. Bengtsson and I. Ragnarsson, Rotational bands and particle-hole excitations at very high spin, *Nucl. Phys. A* 436(1), 14 (1985)
69. W. Reviol, M. P. Carpenter, U. Garg, R. V. F. Janssens, I. Ahmad, I. G. Bearden, P. Benet, P. J. Daly, M. W. Drigert, P. B. Fernandez, T. L. Khoo, E. F. Moore, S. Pilotte, and D. Ye, Shape-driving effects in ^{193}Tl from the spectroscopy of yrast and near-yrast states, *Nucl. Phys. A* 548(2), 331 (1992)
70. C. M. Petrache, D. Bazzacco, S. Lunardi, C. Rossi Alvarez, G. de Angelis, M. de Poli, D. Bucurescu, C. A. Ur, P. B. Semmes, and R. Wyss, Rotational bands in the doubly odd nucleus ^{134}Pr, *Nucl. Phys. A* 597(1), 106 (1996)
71. A. J. Kreiner, M. Fenzl, S. Lunardi, and M. A. Mariscotti, Rotational structures in doubly odd ^{198}Tl, *Nucl. Phys. A* 282(2), 243 (1977)
72. P. Joshi, M. P. Carpenter, D. B. Fossan, T. Koike, E. S. Paul, G. Rainovski, K. Starosta, C. Vaman, and R. Wadsworth, Effect of γ softness on the stability of chiral geometry: Spectroscopy of ^{106}Ag, *Phys. Rev. Lett.* 98(10), 102501 (2007)
73. D. Jerrestam, W. Klamra, J. Gizon, F. Lidén, L. Hildingsson, J. Kownacki, Th. Lindblad, and J. Nyberg, Collective bands in ^{106}Ag and ^{107}Ag, *Nucl. Phys. A* 577(3–4), 786 (1994)
74. H. L. Ma, S. H. Yao, B. G. Dong, X. G. Wu, H. Q. Zhang, and X. Z. Zhang, Risk of misinterpreting nearly degenerate doublet bands as chiral partners in odd–even $^{103,\ 105,\ 107}$Ag and odd–odd ^{106}Ag, *Phys. Rev. C* 88(3), 034322 (2013)
75. J. Peng, H. Sagawa, S. Q. Zhang, J. M. Yao, Y. Zhang, and J. Meng, Search for multiple chiral doublets in rhodium isotopes, *Phys. Rev. C* 77(2), 024309 (2008)
76. J. M. Yao, B. Qi, S. Q. Zhang, J. Peng, S. Y. Wang, and J. Meng, Candidate multiple chiral doublets nucleus ^{106}Rh in a triaxial relativistic mean-field approach with time-odd fields, *Phys. Rev. C* 79(6), 067302 (2009)
77. J. Li, S. Q. Zhang, and J. Meng, Multiple chiral doublet candidate nucleus ^{105}Rh in a relativistic mean-field approach, *Phys. Rev. C* 83(3), 037301 (2011)
78. A. D. Ayangeakaa, U. Garg, M. D. Anthony, S. Frauendorf, J. T. Matta, B. K. Nayak, D. Patel, Q. B. Chen, S. Q. Zhang, P. W. Zhao, B. Qi, J. Meng, R. V. F. Janssens, M. P. Carpenter, C. J. Chiara, F. G. Kondev, T. Lauritsen, D. Seweryniak, S. Zhu, S. S. Ghugre, and R. Palit, Evidence for multiple chiral doublet bands in ^{133}Ce, *Phys. Rev. Lett.* 110(17), 172504 (2013)
79. P. W. Zhao, Z. P. Li, J. M. Yao, and J. Meng, New parametrization for the nuclear covariant energy density

functional with a point-coupling interaction, *Phys. Rev. C* 82(5), 054319 (2010)
80. A. I. Levon, J. de Boer, A. A. Pasternak, and D. A. Volkov, M1-transitions and the mutual orientation of the unpaired nucleons in odd–odd nuclei, *Z. Phys. A* 343(2), 131 (1992)
81. N. Rather, P. Datta, S. Chattopadhyay, S. Rajbanshi, A. Goswami, G. H. Bhat, J. A. Sheikh, S. Roy, R. Palit, S. Pal, S. Saha, J. Sethi, S. Biswas, P. Singh, and H. C. Jain, Exploring the origin of nearly degenerate doublet bands in ^{106}Ag, *Phys. Rev. Lett.* 112(20), 202503 (2014)
82. P. A. Butler and W. Nazarewicz, Intrinsic reflection asymmetry in atomic nuclei, *Rev. Mod. Phys.* 68(2), 349 (1996)
83. B. Ackermann, H. Baltzer, C. Ensel, K. Freitag, V. Grafen, C. Günther, P. Herzog, J. Manns, M. Marten-Tölle, U. Müller, J. Prinz, I. Romanski, R. Tölle, J. deBoer, N. Gollwitzer, and H. J. Maier, Collective E1 transitions in even-A Ra, Th, and U nuclei, *Nucl. Phys. A* 559(1), 61 (1993)
84. P. Mason, G. Benzoni, A. Bracco, F. Camera, B. Million, O. Wieland, S. Leoni, A. K. Singh, A. Al-Khatib, H. Hübel, P. Bringel, A. Bürger, A. Neusser, G. Schönwasser, B. M. Nyakó, J. Timár, A. Algora, Z. Dombrádi, J. Gál, G. Kalinka, J. Molnár, D. Sohler, L. Zolnai, K. Juhász, G. B. Hagemann, C. R. Hansen, B. Herskind, G. Sletten, M. Kmiecik, A. Maj, J. Styczen, K. Zuber, F. Azaiez, K. Hauschild, A. Korichi, A. Lopez-Martens, J. Roccaz, S. Siem, F. Hannachi, J. N. Scheurer, P. Bednarczyk, T. Byrski, D. Curien, O. Dorvaux, G. Duchêne, B. Gall, F. Khalfallah, I. Piqueras, J. Robin, S. B. Patel, O. A. Evans, G. Rainovski, C. M. Petrache, D. Petrache, G. L. Rana, R. Moro, G. D. Angelis, P. Falon, I. Y. Lee, J. C. Lisle, B. Cederwall, K. Lagergen, R. M. Lieder, E. Podsvirova, W. Gast, H. Jäger, N. Redon, and A. Görgen, Evidence for octupole correlations in $^{124,\,125}$Ba, *Phys. Rev. C* 72(6), 064315 (2005)
85. Y. Y. Wang, S. Q. Zhang, P. W. Zhao, and J. Meng, Multiple chiral doublet bands with octupole correlations in reflection-asymmetric triaxial particle rotor model, *Phys. Lett. B* 792, 454 (2019)
86. K. T. Hecht and A. Adler, Generalized seniority for favored $J \neq 0$ pairs in mixed configurations, *Nucl. Phys. A* 137(1), 129 (1969)
87. A. Arima, M. Harvey, and K. Shimizu, Pseudo LS coupling and pseudo $SU(3)$ coupling schemes, *Phys. Lett. B* 30(8), 517 (1969)
88. H. Jia, B. Qi, C. Liu, and S. Y. Wang, Coexistence of chiral symmetry and pseudospin symmetry in one nucleus: Triplet bands in ^{105}Ag, *J. Phys. G* 46(3), 035102 (2019)
89. S. Guo, C. M. Petrache, D. Mengoni, Y. H. Qiang, Y. P. Wang, Y. Y. Wang, J. Meng, Y. K. Wang, S. Q. Zhang, P. W. Zhao, A. Astier, J. G. Wang, H. L. Fan, E. Dupont, B. F. Lv, D. Bazzacco, A. Boso, A. Goasduff, F. Recchia, D. Testov, F. Galtarossa, G. Jaworski, D. R. Napoli, S. Riccetto, M. Siciliano, J. J. Valiente-Dobon, M. L. Liu, G. S. Li, X. H. Zhou, Y. H. Zhang, C. Andreoiu, F. H. Garcia, K. Ortner, K. Whitmore, A. Ataç-Nyberg, T. Bäck, B. Cederwall, E. A. Lawrie, I. Kuti, D. Sohler, T. Marchlewski, J. Srebrny, and A. Tucholski, Evidence for pseudospin-chiral quartet bands in the presence of octupole correlations, *Phys. Lett. B* 807, 135572 (2020)
90. H. Liang, J. Meng, and S. G. Zhou, Hidden pseudospin and spin symmetries and their origins in atomic nuclei, *Phys. Rep.* 570, 1 (2015)
91. Q. Xu, S. J. Zhu, J. H. Hamilton, A. V. Ramayya, J. K. Hwang, B. Qi, J. Meng, J. Peng, Y. X. Luo, J. O. Rasmussen, I. Y. Lee, S. H. Liu, K. Li, J. G. Wang, H. B. Ding, L. Gu, E. Y. Yeoh, and W. C. Ma, Identification of pseudospin partner bands in ^{108}Tc, *Phys. Rev. C* 78(6), 064301 (2008)